運輸省港湾技術研究所

港湾技術研究所報告

REPORT OF THE PORT AND HARBOUR RESEARCH INSTITUTE

MINISTRY OF TRANSPORT

VOL. 30 NO. 2(1) JUNE 1991

NAGASE, YOKOSUKA, JAPAN

港湾技術研究所報告 (REPORT OF P.H.R.I)

第30巻 第2号 (Vol. 30, No. 2) 1991年6月 (June. 1991)

目 次 (CONTENTS)

1. Investigation of Cross-shore Sediment Transport Rates and Flow Parameters in the Surf Zone using Field Data
..... Yoshiaki KURIYAMA 13

(現地データによる砕波帯内の岸沖漂砂量と流速特性の検討
..... 栗山 善昭)

2. 避泊フェリーの係留張力と振れ回り運動に関する検討
..... 平石 哲也・本城 智 59

(Characteristics of the motion and tension of a ferry moored in a storm
..... Tetsuya HIRAISHI and Satoshi HONJYO)

3. 離散渦法による構造物周りの流れシミュレーション
..... 細川 恭史・古川 恵太 155

(Modeling of Discrete Vortices Induced by an Inclined Flat Plate
Yasushi HOSOKAWA and Keita FURUKAWA)

4. プラスティックボードドレーンで改良された不均一地盤の沈下特性
..... 田中 洋行・太田 一己・丸山 隆英 211

(Performance of Vertical Drains for Soft and Ununiform Soils
..... Hiroyuki TANAKA, Kazumi OHTA and Takahide MARUYAMA)

5. 杭の横抵抗における捨石層の評価
..... 高橋 邦夫・壹岐 幸史 229

(Lateral Resistance of a Pile in Rubble Mound
..... Kunio TAKAHASHI and Yukifumi IKKI)

6. サンドドレーンの効果に関する有限要素解析
..... 小林 正樹 275

(Finite Element Analysis of the Effectiveness of Sand Drains
..... Masaki KOBAYASHI)

7. 接円式深層混合処理地盤の挙動
..... 北詰 昌樹・中村 健・寺師 昌明 305

(Reliability of Clay Ground Improved by the Group Column Type DMM with High Replacement)
..... Masaki KITAZUME, Takeshi NAKAMURA and Masaaki TERASHI)

8．斜面近傍の杭頭自由の長杭の横抵抗
…… 寺師　昌明・北詰　昌樹 …… 327
(Influence of a slope on the Lateral Resistance of a Long Pile
…… Masaaki TERASHI and Masaki KITAZUME)

9．液状化による矢板岸壁の変形の数値解析
…… 井合　進・亀岡　知弘 …… 349
(Analysis of Deformation in Sheet Pile Quaywall due to Liquefaction
…… Susumu IAI and Tomohiro KAMEOKA)

10. 盛土の地震被災事例に基づく円形すべり安定解析手法の検討
…… 上部　達生・長田　信 …… 381
(Circular Arc Analysis of Earthquake Damage of Embankments on Saturated Sand Layers
…… Tatsuo UWABE and Makoto OSADA)

11. ねじりを受ける長大ケーソンの力学特性
…… 清宮　理・山田　昌郎 …… 445
(Mechanical Properties of Long Caisson Subjected to Torsion
…… Osamu KIYOMIYA and Masao YAMADA)

12. 歩行式水中調査ロボットの開発
— (第2報) 軽量防水型実験機の設計 —
…… 朝倉　修・秋園　純一・岩崎　峯夫・根本　孝志 …… 483
(Development on Aquatic Walking Robot for Underwater Inspection
– (Second Report) Design of the Light-weight Type Aquatic Walking Robot –
…… Osamu ASAKURA, Jun-ichi AKIZONO, Mineo IWASAKI and Takashi NEMOTO)

13. 水平管における空気混入軟泥の流動特性
…… 岡山　義邦・鮎貝　基和・鈴木　誠・福本　裕哉 …… 533
(Fluidity Characteristics of Muddy Slurry with Compressed Air in Horizontal Plipe
…… Yoshikuni OKAYAMA, Motokazu AYUGAI, Makoto SUZUKI and Hiroya FUKUMOTO)

REPORT OF THE PORT AND
HARBOUR RESEARCH INSTITUTE
Vol. 30, No. 2 (June 1991)

Investigation of Cross-shore Sediment Transport Rates and Flow Parameters in the Surf Zone using Field Data

Yoshiaki KURIYAMA*

Synopsis

Field measurements have been carried out by using a 427m long pier in high and low wave conditions. Horizontal current velocities and surface elevations were measured for twenty minutes every two hours at one or two stations in each series of measurements. A series of measurements was continued about two weeks. Breaker properties such as breaker type and breaking position were visually observed several times a day. The bottom profiles along the pier were also measured once a day.

Two different mechanisms of sediment transport are shown to be dominant in the surf zone. One is the transport of the sediments which are suspended by the turbulence due to wave breaking and transported by the time-averaged cross-shore velocities. The other is the sediment transport in the vicinity of ripples. As a result, time-averaged cross-shore velocities, the root-mean-square values of the velocities along the principal wave direction and the forward asymmetry of the velocities are strongly related to the cross-shore sediment transport rates in the surf zone. The new relationship between the cross-shore sediment transport rate and the flow parameters is valid not only near wave breaking positions but also in the middle of the surf zone when the erosion volume in the foreshore is small. However, it cannot hold good even near wave breaking positions when the erosion volume in the foreshore is large.

The theoretical prediction formula for the time-averaged cross-shore velocity derived by *Svendsen* (1984) is improved for irregular waves with the introduction of the fraction of breaking waves and the root-mean-square value of water surface elevation. The improved formula consists of two terms as Svendsen's model does. One is the velocity due to the surface variations; this term is verified with the field data outside the surf zone. The other is the velocity due to the turbulence generated by wave breaking. The surface roller area parameter, which is the nondimensionalized velocity due to the turbulence, decreases as the distance from the wave breaking position to the measurement station increases. This parameter increases in the zone where bores fully develop as the ratio of the plunging breakers to all breakers increases. The square-root-mean value of the orbital velocity is 0.8 times as much as the value predicted with the root-mean-square value of the surface elevation using the small amplitude wave theory. The atiltness of the velocity, which expresses the forward asymmetry, is strongly related to the wave nonlinearity parameter proposed by *Goda* (1983). The atiltness increases as the parameter increases in the range from 0.3 to 4.

Key Words: Field Measurement, Time-averaged Cross-shore Velocity, Orbital Velocity, Atiltness, Cross-shore Sediment Transport Rate, HORF

* Member of Littoral Drift Laboratory, Hydraulic Engineering Division

港湾技術研究所報告
第30巻第2号 (1991.6)

現地データによる砕波帯内の岸沖漂砂量と流速特性の検討

栗山　善昭*

要　旨

砕波帯内における岸沖漂砂量と流速特性との関係、および流速特性と水面変動との関係を検討するために、長さ427m の波崎海洋研究施設（HORF）において約２週間の現地観測を４回行なった。沿岸流速、岸沖流速ならびに水面変動を、１地点あるいは２地点で２時間に１回、20分間測定し、砕波位置、砕波形式、砕波率、離岸流の位置を１日数回、観察した。施設に沿った断面は、１日１回、レッドなどを使って5m間隔で測定した。

３つの底質移動形態を仮定し、それぞれの岸沖漂砂量を評価したところ、砕波帯内では砕波で生じた乱れによって浮遊し時間平均の沖向き流速によって運ばれる底質移動と、リップル周辺の底質移動が卓越していた。その結果、時間平均の沖向き流速、波の主方向の振動流成分、ならびに流速波形の前後の非対称性が砕波帯内の岸沖漂砂量と強く結びついていた。本論文で見いだされた岸沖漂砂量と流速特性との関係は、前浜の地形変化が小さい場合には、砕波位置近傍のみならず砕波帯中程でも成り立った。しかし、前浜の地形変化が大きい場合にはこの関係が成り立たなかった。

Svendsen (1984)によって導かれた沖向き時間平均流速の理論式を不規則波にも適用できるように砕波率と水面変動のrms値を導入して改良した。波動成分による流れの項の妥当性は砕波帯外の実測データによって確認された。ボアによる流れを波高等で無次元化した値は、砕波位置から遠ざかるほど小さくなり、ボアが十分発達した領域では巻き波砕波の割合が大きいほどその値が大きくなった。

波の主方向の流速成分のrms値は、微小振幅波理論を使って水面変動のrms値から計算される値の約0.8倍であった。

波の主方向の流速変動の前後の非対称性を表わすatiltnessは、合田（1983）によって提案された波の非線形性を表わすパラメーター$\Pi_{1/3}$との相関が強く、$\Pi_{1/3}$が0.3 から4 の範囲で増加するにしたがってatiltnessは大きくなった。

キーワード；現地観測、沖向き時間平均流速、
振動流成分、atiltness、岸沖漂砂量、
HORF

*水工部　漂砂研究室

Contents

Synopsis 3

1. Introduction 7

2. Outline of field measurements 7
2.1 Study site, and measuring items and procedure 7
2.2 Calibrations of electro-magnetic current meter 11

3. Wave conditions and bottom profile changes 13

4. Relationships between cross-shore sediment transport rates and flow parameters 28

5. Relationships between flow parameters and wave parameters 41
5.1 Time-averaged cross-shore velocities 41
5.2 Orbital velocities 49
5.3 Velocity atiltness 50

6. Conclusions 51

Acknowledgments 52

References 53

List of Symbols 54

Appendix A. Wave profile atiltness 56

Appendix B. Wave profile skewness and velocity skewness 56

1. Introduction

Artificially nourished beaches have been constructed at many places in Japan for maritime recreation and disaster prevention. In the planning and design of sandy beaches, one needs to predict future changes of beach profile due to cross-shore sediment transport. Although there are a great number of cross-shore sediment transport formulas such as those listed by *Kajima and Katori* (1988), the reliable formula is still absent. Therefore the prediction often relies on engineer's experience.

One of the causes for the absence of the reliable formula is the lack of verification with the field data. Most of the proposed formulas are based on the laboratory data. The formulas should be verified with field data since there is no similarity law for sand transport rates. However, the verifications were seldom carried out because the field data such as cross-shore sediment transport rates and cross-shore velocities are difficult to obtain especially in storm conditions.

Another cause is that one cannot determine the wave parameters which should be used in the formula because of an imperfect understanding of the complicated cross-shore sand transport. The importance of the following factors to the cross-shore sediment transport have been recognized: return flows (*Dally and Dean*, 1984), the turbulence due to wave breaking (*Nadaoka et al.*, 1988), the upward asymmetry of the velocity along the principal wave direction (*Bowen*, 1980; *Bailard*, 1982), and the forward asymmetry of the velocity (*Katoh et al.*, 1985). However, the contribution rates of the factors to the cross-shore sediment transport rates are not thoroughly assessed.

Therefore the relationships between the cross-shore sediment transport rates and the flow parameters are investigated by examining the contribution rates of the factors with field data. Field measurements at a field observation pier have been carried out in high and low wave conditions.

The measuring procedure and the properties of the utilized instruments are presented in Chapter 2. The wave conditions and the beach profile changes are described in Chapter 3. In Chapter 4, the relationships between cross-shore sediment transport rates and various flow parameters are represented. Methods of estimating the flow parameters which are strongly related to the cross-shore sediment transport rates are investigated with the wave parameters such as the wave height, the wave period and the wave nonlinearity parameter in Chapter 5.

2. Outline of field measurements

2.1 Study site, and measuring items and procedure

Four series of field measurements have been carried out at the Hazaki Oceanographical Research Facility (HORF) facing to the Pacific Ocean (Fig.1). The HORF is the pier 427m long for field observations in the nearshore zone. Figure 2 shows the side view of the HORF and the mean profile in 1987. The horizontal axis expresses the offshoreward distance from the reference point near the entrance of the HORF. The mark "P" is defined to indicate a point; for example, the mark "P145m" indicates the point where the offshore distance from the reference point is 145m. The working platform of the HORF is 393m long, 3.3m wide and 6.9m above the low water level. The average beach slope along the HORF is about 1/60. A trough frequently exists in the region from P190m to P220m, and a bar crest is located near P300m. The median sediment diameter is 0.18mm although it varied from 0.2mm to 1.0mm at a trough (*Katoh et al.*,1990).

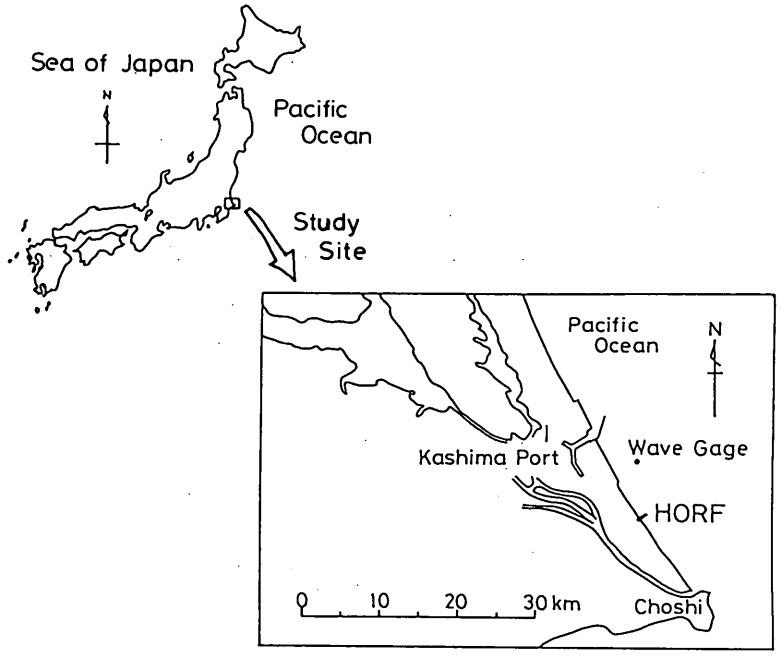

Fig.1 Study site

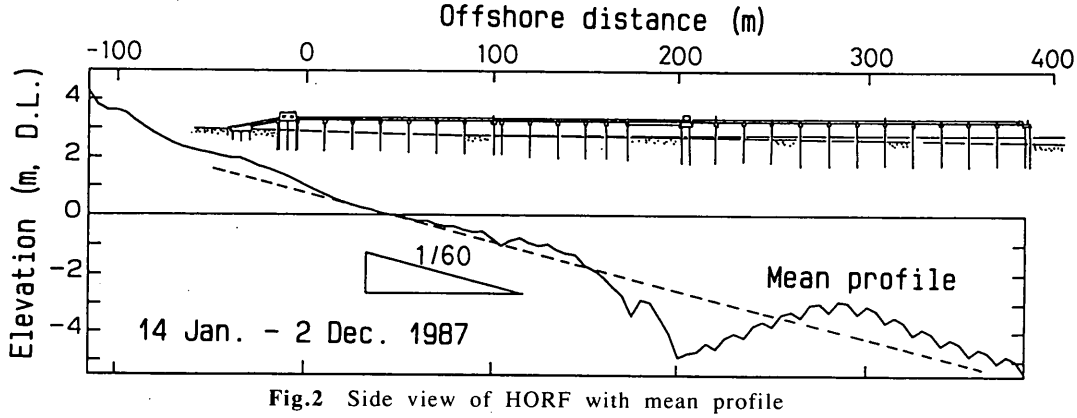

Fig.2 Side view of HORF with mean profile

The duration, the utilized instruments and the measurement stations, where the instruments were installed, are summarized in Table 1 for four series of field measurements, which are called as Measurement A,B,C and D. Measurement A and B were carried out near the wave breaking positions in different wave conditions. Measurement C was conducted in the middle of the surf zone in a storm. At Measurement D, instruments were installed near the wave breaking positions and in the middle of the surf zone. Horizontal current velocities were measured with electro-magnetic current meters of two-component type. Water surface elevations were measured with ultrasonic wave gages, which had already been installed at the south side of the platform. At the measurement station, usually one current meter was installed while three current meters were installed vertically at P145m during Measurement B. Table 2 indicates the properties of the instruments utilized in the measurements. The current meters at P145m were mounted on a ladder as shown in Fig.3. One end of the ladder is fixed to the platform,

Table 1 Duration and station of measurement, and instrument

Measurement name	Duration	Station		Instrument	
Measurement A	Sep. 12 – Sep. 26, 1988	P145m		EMC B*1	USW*2
Measurement B	July 13 – July 21, 1989	P145 m	Upper	EMC B	USW
			Middle	EMC A	
			Lower	EMC D	
Measurement C	Feb. 9 – Feb. 28, 1990	P80m		EMC C	USW
		P50m		EMC A	—
Measurement D	June 25 – July 10, 1990	P145m		EMC B	USW
		P80m		EMC C	USW

*1 EMC : Electro magnetic current meter
*2 USW : Ultrasonic wave gage

Table 2 Property of utilized instrument

Instrument name	Model number	Measurement range	Output voltage	Response time
EMC A	Yokogawa Navitec: model EMC 101	3m/s	0.333v/(m/s)	0.1s
EMC B EMC C	Alec model ACM 200 PC	6m/s	1v/(m/s)	0.05s
EMC D	Kenec model VMT2-200-08P	3m/s	1.67v/(m/s)	0.05s
USW	Kenec model UHT2-10	10 m	0.5v/m	less than 0.1s

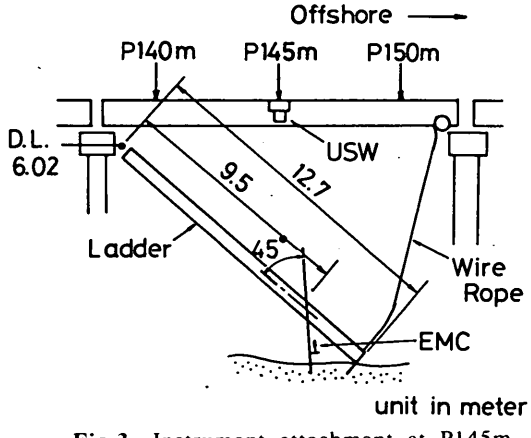

Fig.3 Instrument attachment at P145m

while the other end is pulled up with a wire rope. After the attachment of instruments to the ladder, the wire rope is released gently until the ladder end reaches the seabed; this avoids the need for underwater doing. At P80m and P50m, current meters were mounted to pipes as shown in Fig.4.

Water surface elevations and horizontal velocities were measured for twenty minutes at a sampling frequency of 2Hz. The data were transmitted through a cable to the micro-computer in an observation room near the entrance of the HORF, and were recorded

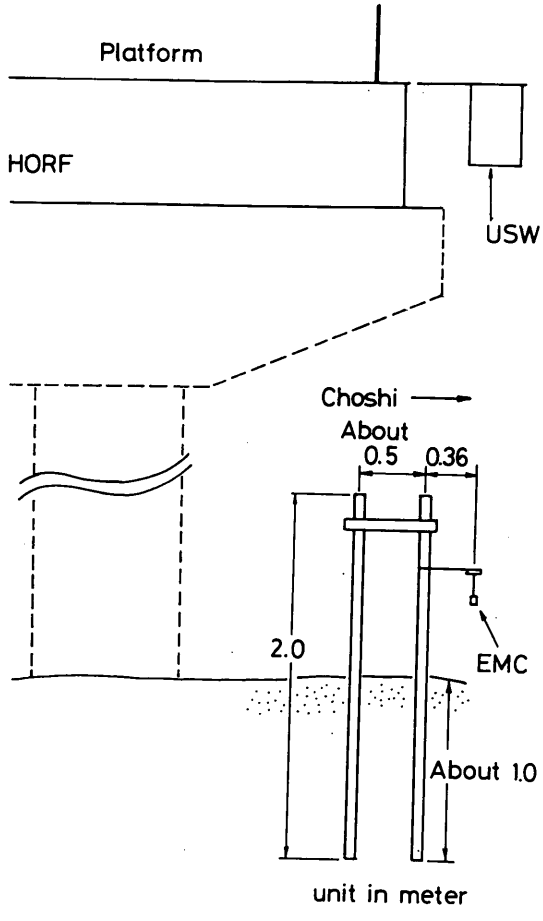

Fig.4 Instrument attachment at P80m and P50m

Table 3 Burst interval

Burst interval	Period
Fourty minutes	1620 Sep. 14 – 1240 Sep. 17, 1988
One hour	1245 Sep. 17 – 1730 Sep. 19, 1988
	0050 Feb. 9 – 1730 Feb. 9, 1990
	1050 Feb. 13 – 1730 Feb. 13, 1990
	0950 Feb. 14 – 1130 Feb. 17, 1990
	1050 Feb. 19 – 1730 Feb. 19, 1990
	1050 Feb. 20 – 1730 Feb. 20, 1990
	1050 Feb. 21 – 1730 Feb. 22, 1990
	0950 Feb. 23 – 1730 Feb. 23, 1990
	0950 Feb. 26 – 1730 Feb. 26, 1990
	0950 Feb. 27 – 1730 Feb. 27, 1990
	0950 Feb. 28 – 1530 Feb. 28, 1990
Two hours	except for the periods described above

on magnetic tapes after A/D conversion. Although most of the burst intervals were two hours, they were one hour and forty minutes at some periods as described in Table 3.

Spikes in the data were found out by inspecting the graphic charts of the time series of the data. When the number of the spikes in a data set of a measuring item for twenty minutes is less than ten, each spike is replaced by the average of the values before and after the spike. However, a data set including more than ten spikes is abandoned.

Figure 5 shows the co-ordinate system used in this paper. The positive directions of cross-shore velocity and longshore velocity are seaward and southward, respectively. The vertical axis extends upwards. Elevations are relative to a datum level in Hasaki. The wave direction is defined relative to the shoreward direction and positive in counterclockwise.

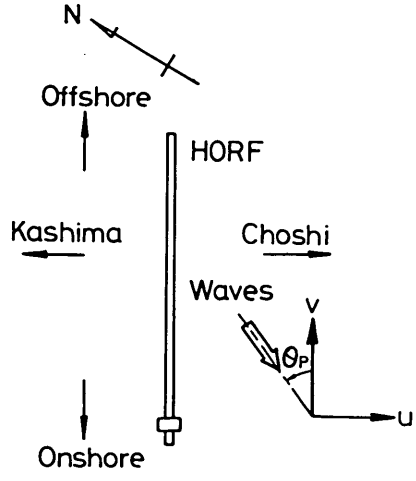

Fig.5 Definition sketch of co-ordinate system

Visual observations for about five minutes were carried out several times in a day in order to observe a fraction of breaking waves, the ratio of plunging breakers to all breakers, the wave breaking positions, the locations of the shorelines, and the presence of rip currents. The strong seaward movement of air bubbles on the surface or that of turbid water with a lot of suspended sand, whose color is brown, was judged as a rip current.

The levels of current meters and those of the sea bottom on both sides of the platform at the measurement stations were measured with a 5kg lead weight after the visual observations.

The beach profiles along the south side of the platform have been measured every 5m once a day except for holidays. The region from P-115m to P-5m have been measured with a level and a staff while the bottom profile from P0m to P385m has been measured with the lead.

The beach profiles on the foreshore were surveyed every 5m with the level and the staff before and after a series of measurements. The profiles were 40m apart, about 200m long, and extended over a longshore distance of 400m.

2.2 Calibrations of electro-magnetic current meters

The offset of an electro-magnetic current meter, which is the output voltage with zero flow velocity, varies during a series of measurements. One of the main reasons

of the drift in the offset is the adhesion of sea organisms to the electrodes of the meter. Precalibration and postcalibration with zero flow velocity were carried out. Since there was a voltage difference between the sea below the platform and the water in a bucket on the platform, the calibrations were conducted in the sea. In order to make the zero flow velocity field around the meter, the meter was surrounded with a wooden box, which is full of sea water. The clearance between a wall of the box and a electrode of the meter was over 20cm to decrease the effect of the wall to the electrode negligibly.

In Table 4, the offsets before and after the series of measurements, and the absolute values of the drifts are listed. The drifts were disregarded since the drifts of EMC A, which are larger than those of the other meters, are within 0.06m/s. The offsets of EMC B after Measurement A and those of EMC C after Measurement C could not

Table 4 Offset before and after the series of measurements, and drift in offset

Measurement name	Station	Instrument name		Offset (mV)		Absolute value of drift in offset	
				Before the series of measurements	After the series of measurements	Unit in mV	Unit in cm/s
Measurement A	P145m	EMC B	X	-4.7	—	—	—
			Y	3.1	—	—	—
Measurement B	P145m Upper	EMC B	X	8.3	-7.3	15.6	1.6
			Y	46.7	27.7	19.0	1.9
	P145m Middle	EMC A	X	33.3	53.4	20.1	6.0
			Y	7.4	25.2	17.8	5.3
	P145m Lower	EMC D	X	-3.7	1.7	5.4	0.3
			Y	46.7	35.7	11.0	0.7
Measurement C	P80m	EMC C	X	0.1	—	—	—
			Y	-4.4	—	—	—
	P50m	EMC A	X	0.7	17.3	16.6	5.0
			Y	-0.9	-11.4	10.5	3.2
Measurement D	P145m	EMC B	X	-6.6	17.7	24.3	2.4
			Y	16.0	33.0	17.0	1.7
	P80m	EMC C	X	-13.4	-7.7	5.7	0.6
			Y	25.4	6.7	18.7	1.9

be measured. The drifts, however, are assumed to be negligible since organisms were considered not to be able to adhere to the sensors because much sand moved and rubbed the sensors owing to severe sea conditions.

The gains of the meters were not recalibrated during these series of measurements since they had been already calibrated in a flow tank in advance.

The offshore wave profiles have been measured at about 7km north from the HORF with an ultrasonic wave gage fixed on the bottom, where the water depth is 23.4m below the datum level (Fig.1).

3. Wave conditions and beach topography changes

[Measurement A]

Figure 6(1) shows the significant wave heights and the significant wave periods. They are calculated by using the zero-downcrossing method. The significant wave height started to increase on the 13th owing to a typhoon. It reached a maximum of 5.4m on the 16th, when the typhoon was the closest to the HORF. As the typhoon

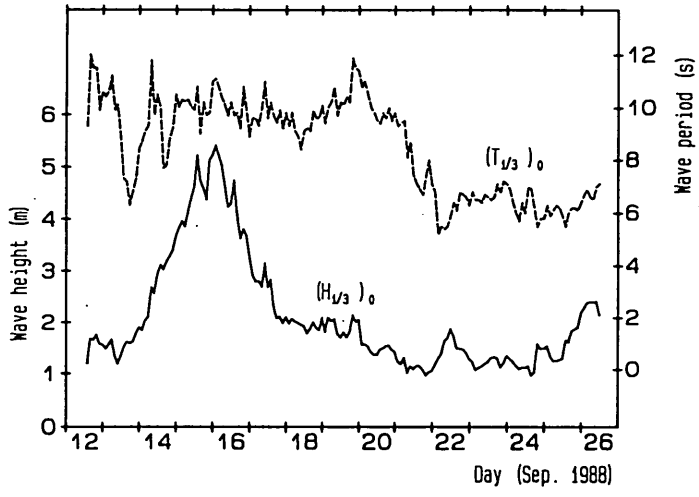

Fig.6(1) Offshore wave heights and wave periods (Measurement A)

moved away from the HORF, the wave heights rapidly decreased to 2.0m. From the 18th to the 25th, the heights were less than 2m. The significant wave periods were about 10s from the 12th to the 17th owing to the swells generated by the typhoon. They were also about 10s from the 17th to the 20th although the wave heights were small from the 18th. On the 21st, the periods started to decrease, and were about 7s from the 22nd to the 26th.

Figure 6(2) shows the wave breaking positions and breaker types. A circle represents

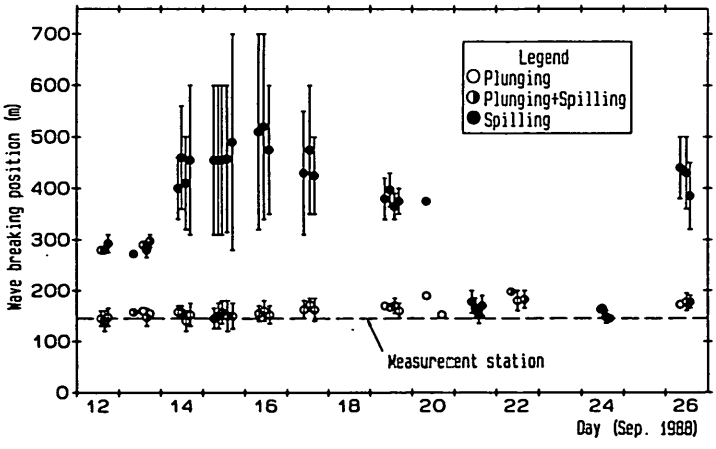

Fig.6(2) Wave breaking positions and breaker types (Measurement A)

a plunging breaker type, in which the ratio of plunging breakers to all breakers observed visually was more than 0.6. A black circle represents a spilling breaker type, in which the ratio was less than 0.4, while a half-black circle represents a ratio between 0.4 and 0.6. The solid line vertically extending across the circle indicates the level of fluctuation of the wave breaking positions during a visual observation. The wave breaking positions over P400m were not observed accurately because the tip of the HORF is located at P385m. The dashed line expresses the measurement station, where a current meter was installed. Waves broke twice during the series of measurements except for the time period when the wave heights were small, from the 21st to the 24th. The offshore breaking positions moved seaward as the wave heights increased. The predominant offshore breaker type was spilling. After waves reformed at the trough around P260m, they broke in the region from P140m to P200m in plunging breaker type. The changes of the second breaker positions were small.

Figure 6(3) shows the levels of the electro-magnetic current meter, the tide and the seabed at the measurement station P145m. The horizontal velocities could be measured during the series of measurements since the current meter was not out of sea water.

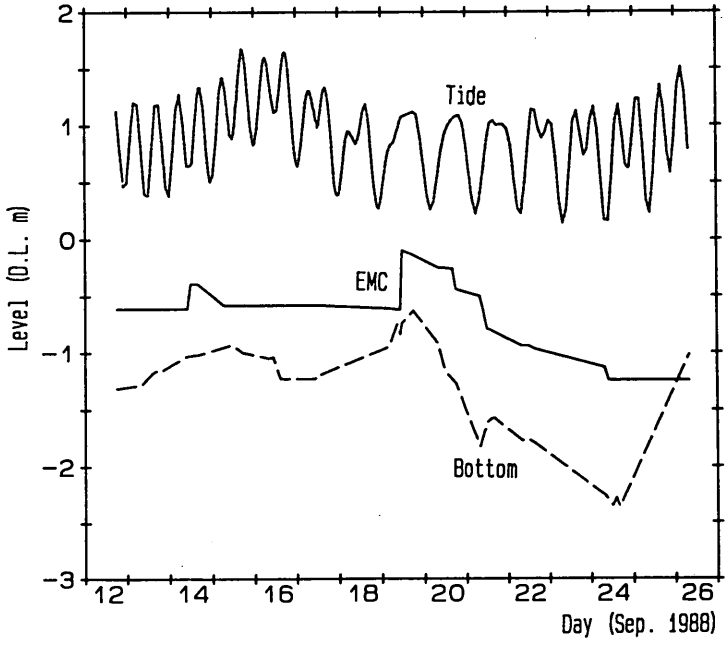

Fig.6(3) Levels of electro-magnetic current meter, tide and the bottom at P145m (Measurement A)

The principal wave direction, θ_p, is defined as

$$\tan 2(\theta_p - \frac{\pi}{2}) = \frac{2\overline{(u-\bar{u})(v-\bar{v})}}{\overline{(u-\bar{u})^2} - \overline{(v-\bar{v})^2}} \qquad (1)$$

where u is the longshore velocity, v is the cross-shore velocity, and the overbar denotes time-averaging.

The upper figure of Fig.6(4) shows the principal wave directions, and the lower one shows the longshore current velocities. Swells due to the typhoon came from

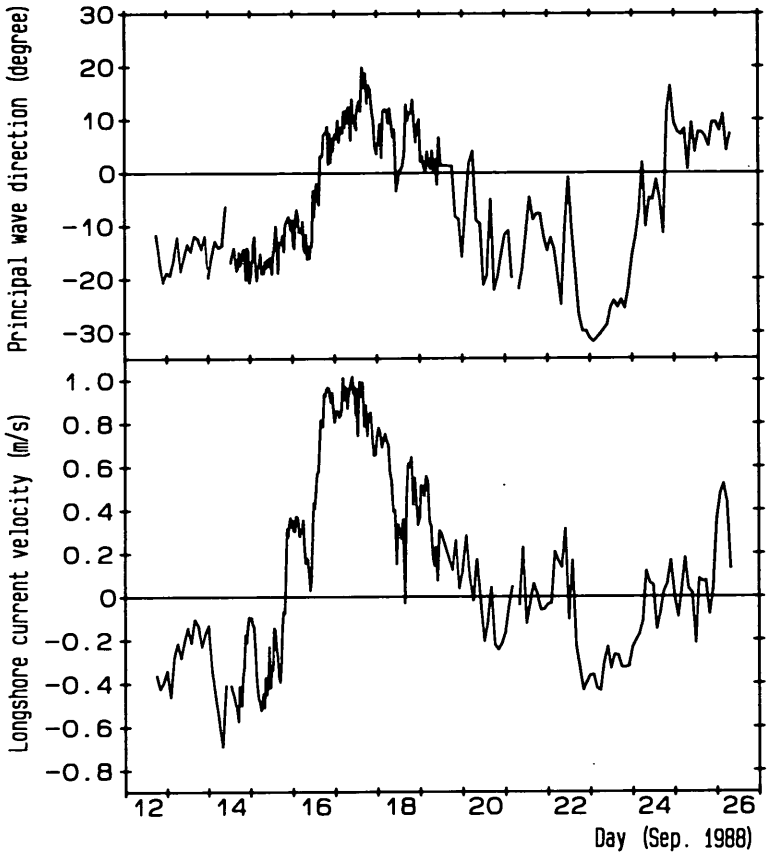

Fig.6(4) Principal wave directions and longshore current velocities (Measurement A)

south on the 13th. As the typhoon moved from south to north, the principal directions changed. Accordingly, the directions of the longshore velocities also changed. On the 17th, the longshore velocity reached a maximum of 1m/s.

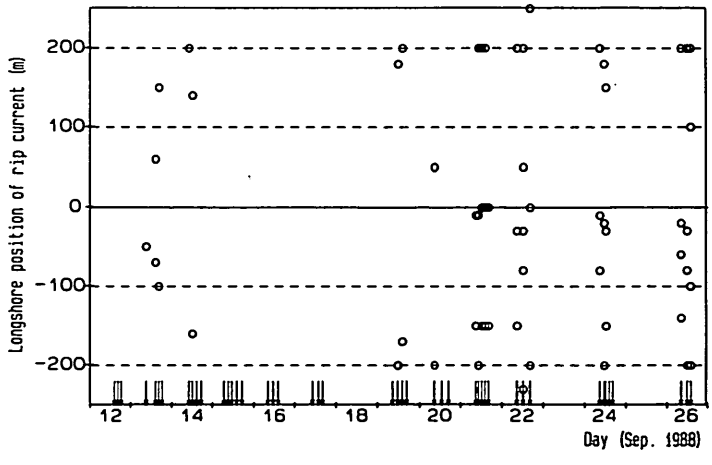

Fig.6(5) Positions of rip currents (Measurement A)

Figure 6(5) shows the longshore positions of rip currents. Arrows in the figure indicate the time when the visual observations were carried out. From the 14th to the 19th, rip currents did not occur near the HORF. However, a rip current occurred 50m away from the HORF on the 20th, and from the 21st rip currents usually occurred near the HORF.

Figure 6(6) shows the beach profile change during the series of measurements. The dashed line and the solid line express the beach profiles before and after the series of measurements, respectively. The foreshore region was eroded owing to the typhoon. The region including the measurement station was also eroded; the sediments accumulated around P200m and formed a bar. The region between P250m and P385m was eroded. The erosion is considered to have occurred owing to the seaward migration of the bar, whose top was located near P300m before the start of the series of measurements.

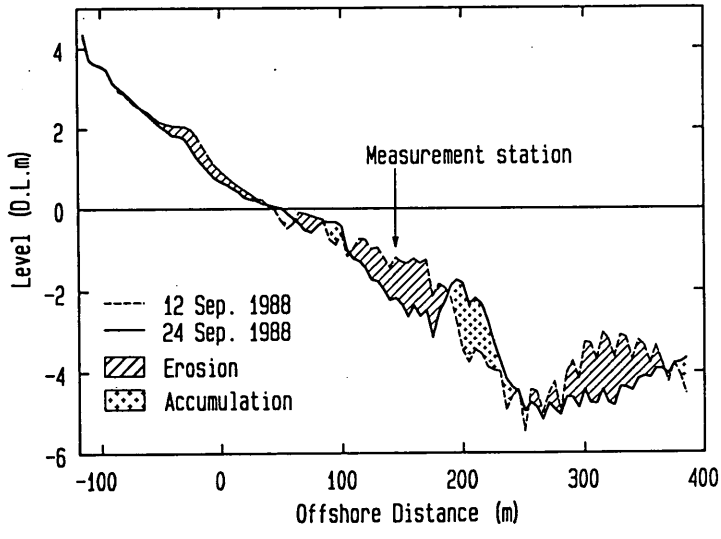

Fig.6(6) Beach profile change (Measurement A)

Figure 6(7) shows the changes of the foreshore topography in the shoreward region of P100m. Although the contour lines of D.L.1m and D.L.2m during the series of measurements were straight as shown in Fig.6(7), the contour lines of D.L.0m were sinuous alongshore. However, the amplitudes of the undulations were small.

[Measurement B]

Figure 7(1) shows the variation of the significant wave heights and the significant wave periods over the duration of the series of measurements. The significant wave heights were small because a high atmospheric pressure extensively covered the Pacific Ocean near Japan. The maximum height was 1.4m. The significant wave periods were about 7s during the series of measurements.

Figure 7(2) shows the wave breaking positions and breaker types. Many of waves broke once on the measurement station or seaward of the station because the wave heights were small. The predominant breaker type was plunging. The wave breaking positions moved shoreward as the mean water levels increased.

Figure 7(3) shows the levels of the electro-magnetic current meter, the tide and the bottom at the measurement station P145m. Since the lower current meter was buried under the bottom from the 18th to the 21th, the horizontal velocities sometimes could not be measured with the lower one.

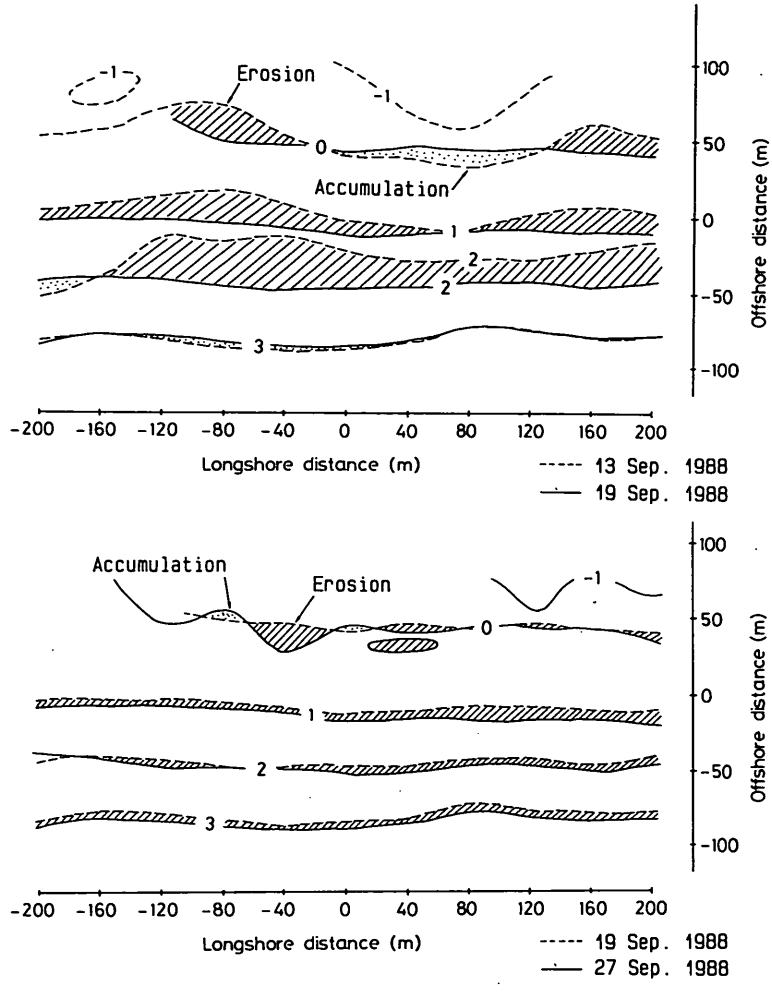

Fig.6(7) Foreshore topography changes (Measurement A)

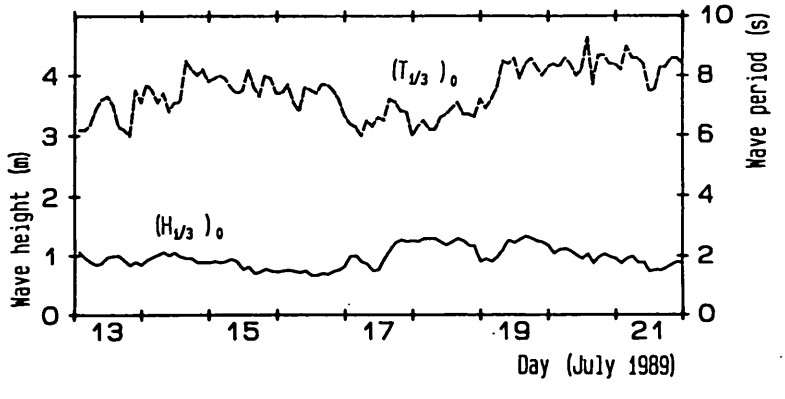

Fig.7(1) Offshore wave heights and wave periods (Measurement B)

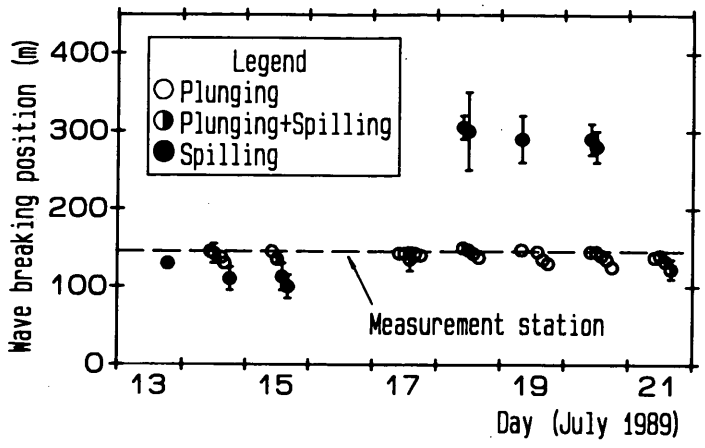

Fig.7(2) Wave breaking positions and breaker types (Measurement B)

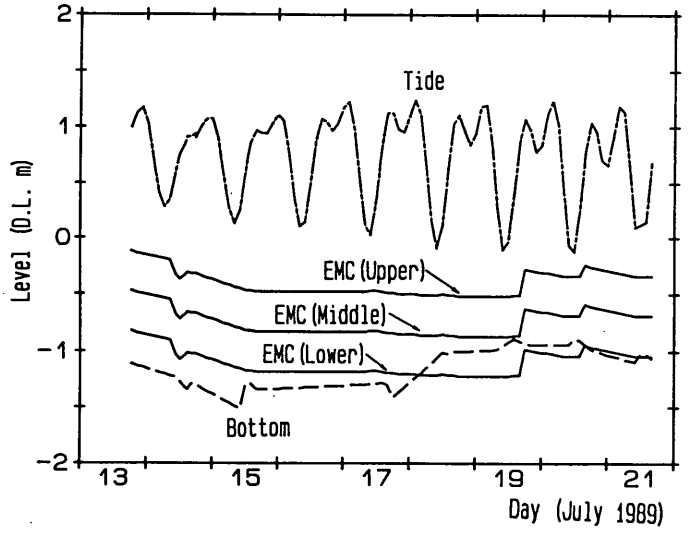

Fig.7(3) Levels of electro-magnetic current meter, tide and the bottom at P145m (Measurement B)

The upper figure of Fig.7(4) shows the principal wave directions, and the lower one shows the longshore current velocities. Waves came from south during the series of measurements. The principal directions measured with the middle current meter were 10 degree larger than those measured by the upper and lower meter. The cause for the difference is suspected to be a misalignment of the middle current meter. However, the difference resulted in errors of less than 0.05m/s in the cross-shore and longshore velocities. Consequently, the velocities measured by the middle current meter are not modified.

The longshore velocities were mostly from south to north owing to the obliquely incident waves, and the absolute values of the velocities are less than 0.4m/s. The differences between those measured with the three meters are mostly less than 0.1m/s while they are nearly equal to 0.3m/s on the 13th. A strong rip current did not occur near the HORF.

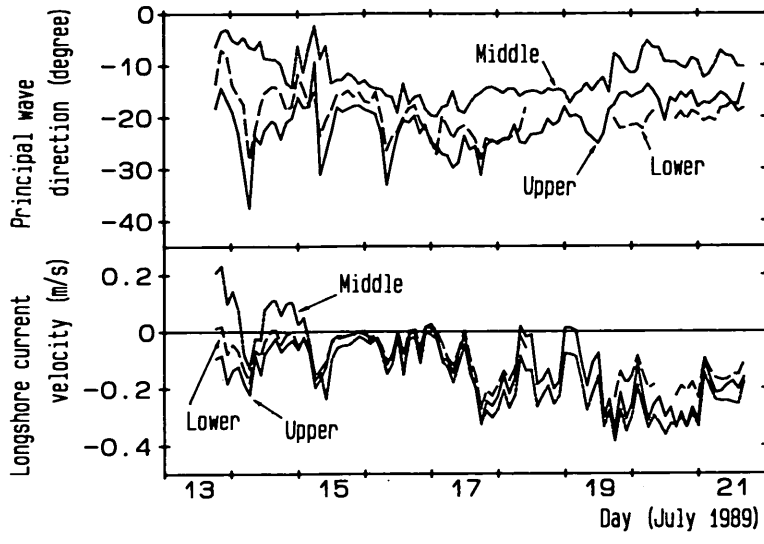

Fig.7(4) Principal wave directions and longshore current velocities (Measurement B)

Figure 7(5) shows the beach profile change. In the region shoreward of the measurement station, sediment accumulation occurred while the seaward region was eroded. The rate of beach profile change was small owing to the low waves.

Figure 7(6) shows the changes of the foreshore topography. The foreshore topography on the 4th was uniform alongshore. Although the contour lines of D.L.1m and D.L.2m on the 19th were linear, the contour line of D.L.0m was sinuous. The cross-shore positions of D.L.0m in the area where the longshore distance from the HORF to the measuring point is between 40m and 80m regressed 40m from the cross-shore positions of D.L.0m in the other areas.

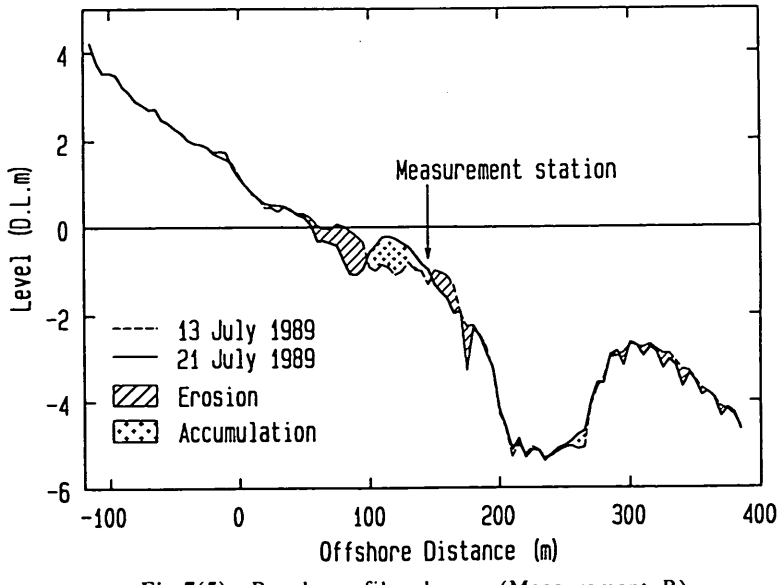

Fig.7(5) Beach profile change (Measurement B)

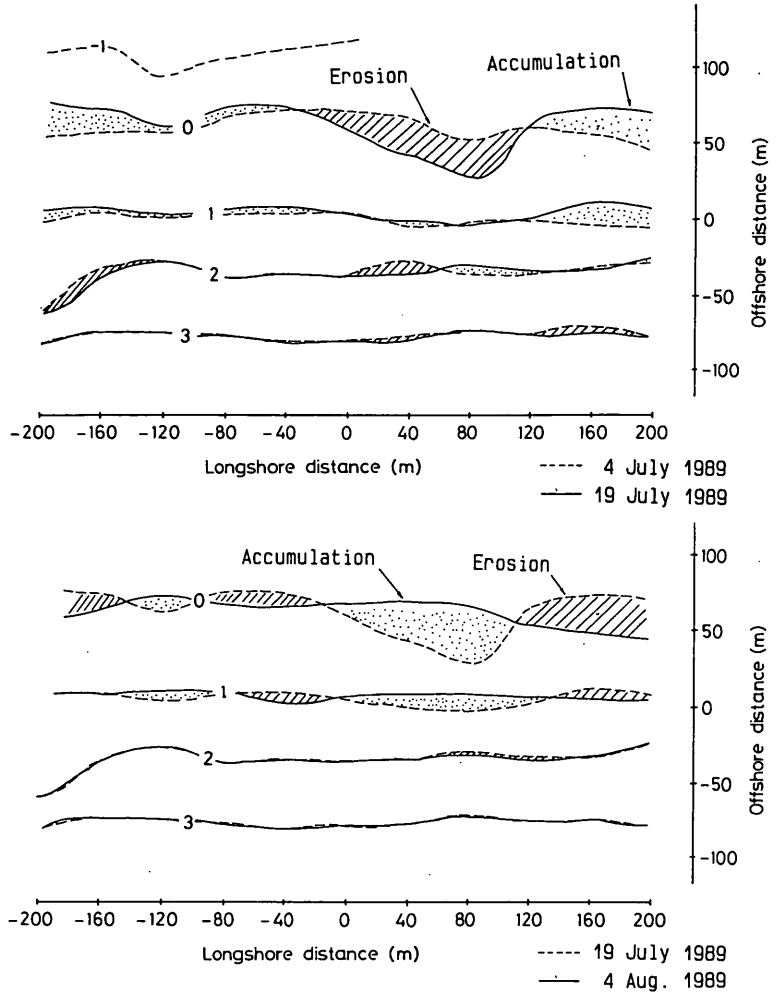

Fig.7(6) Foreshore topography changes (Measurement B)

[Measurement C]

Three low atmospheric pressures passed near the HORF during the series of measurements. Figure 8(1) shows the significant wave heights and the significant wave periods. Although the significant wave heights gradually decreased from the 9th to the 13th, they rapidly increased on the 14th and reached 3.5m on the 15th owing to the first low pressure. On the 17th, the wave heights decreased. They started to increase on the 19th as the second low pressure moved toward the HORF. After reaching a maximum of 2.9m on the 20th, they decreased to 1.0m. The wave heights increased again from the 24th owing to the third one, and were around 2.2m on the 27th. The significant wave periods were mostly less than 10s.

Figure 8(2) shows the wave breaking positions and breaker types. The waves usually broke more than twice. When wave breaking occurred three times, the waves broke twice successively in the seaward region of P190m without reforming. The most offshore breaking positions shifted seaward as the wave heights increased. The predominant offshore breaker type was spilling. Waves reformed at the trough around

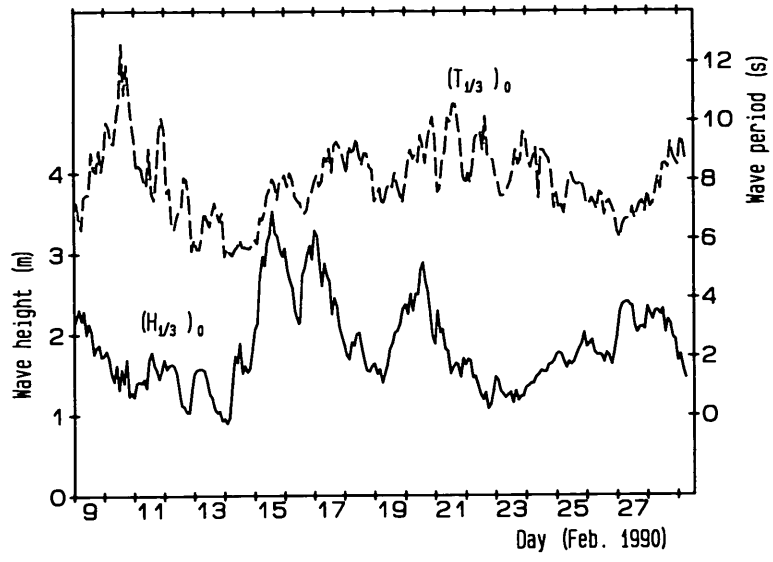

Fig.8(1) Offshore wave heights and wave periods (Measurement C)

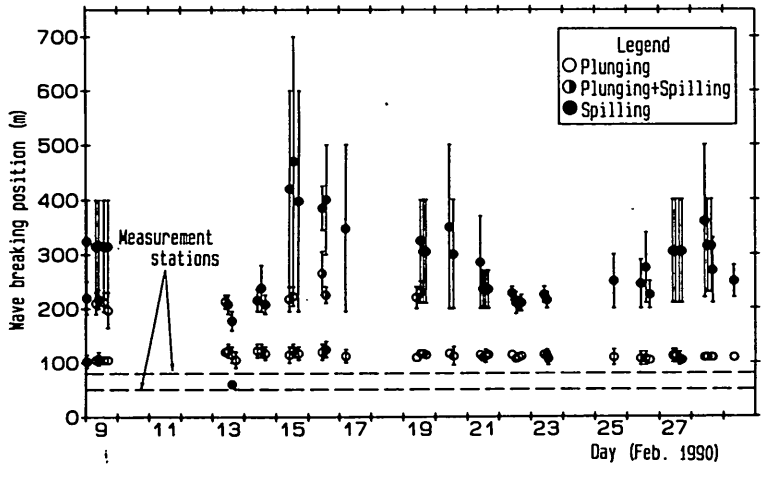

Fig.8(2) Wave breaking positions and breaker types (Measurement C)

P160m. The nearshore breaking positions were fixed, and the predominant nearshore breaker type was plunging. The measurement stations P80m and P50m were in the shoreward region of the nearshore breaking positions.

Figure 8(3) shows the levels of the electro-magnetic current meter, the tide and the bottom at the measurement station P80m, and Fig.8(4) shows those at P50m. The horizontal velocities at the measurement stations could not be measured sometimes because the current meters were out of sea water or buried under the seabed. The current meter at P80m stopped functioning after the 17th.

The upper figure of Fig. 8(5) shows the principal wave directions, and the lower one shows the longshore current velocities. The principal wave directions at the measurement stations, which were located near the shoreline, were less than 10 degree owing to

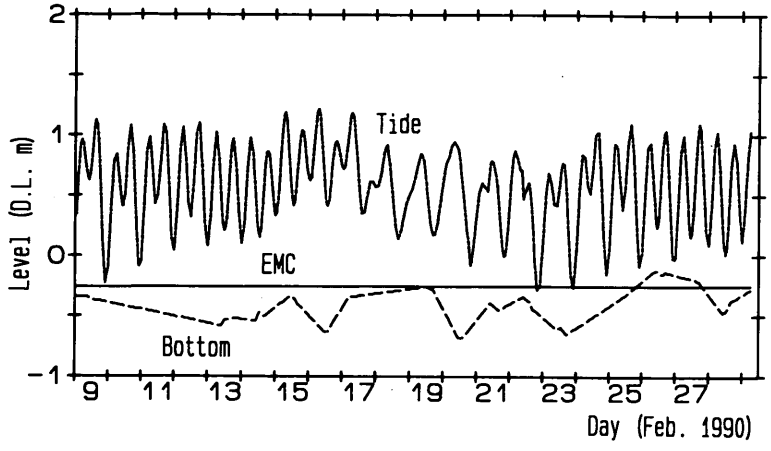

Fig.8(3) Levels of electro-magnetic current meter, tide and the bottom at P80m (Measurement C)

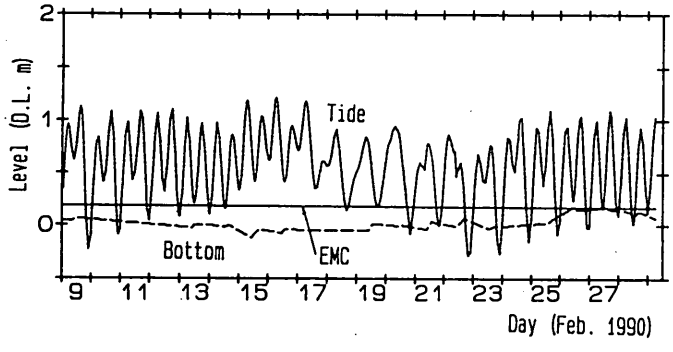

Fig.8(4) Levels of electro-magnetic current meter, tide and the bottom at P50m (Measurement C)

wave refraction. The longshore currents were not small because the wave heights were large. They were sometimes over 0.5m/s. During the series of measurements, a strong rip current did not occur near the HORF.

Figure 8(6) shows the beach profile change. The area between P160m and P230m was eroded, while sediments accumulated in the area between P130m and P160m, and between P-50m and P115m.

Figure 8(7) shows the change of the foreshore topography. The foreshore topography during the series of measurements was uniform alongshore.

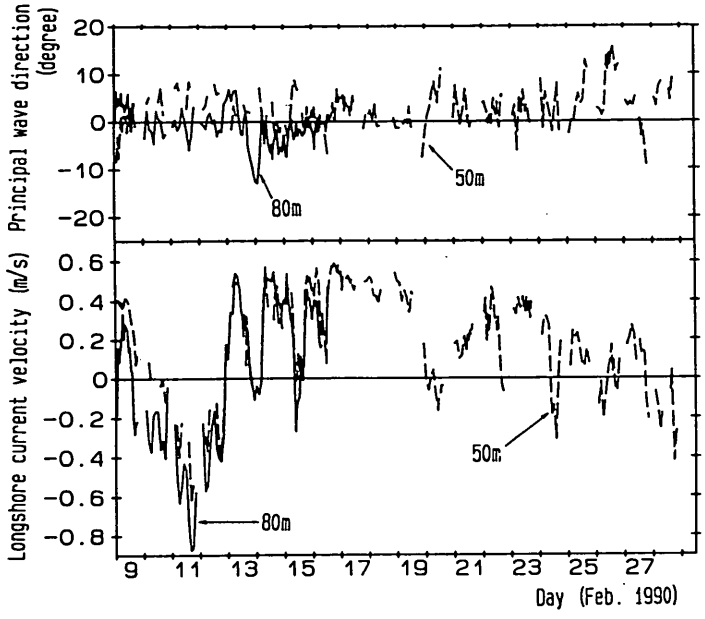

Fig.8(5) Principal wave directions and longshore current velocities (Measurement C)

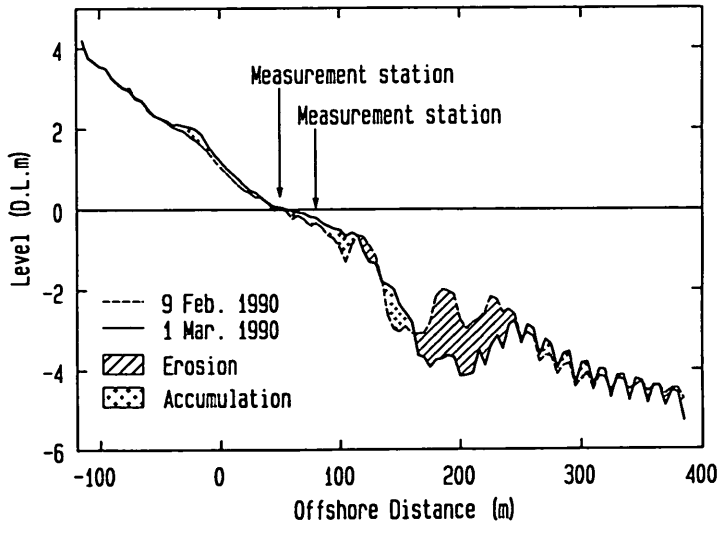

Fig.8(6) Beach profile change (Measurement C)

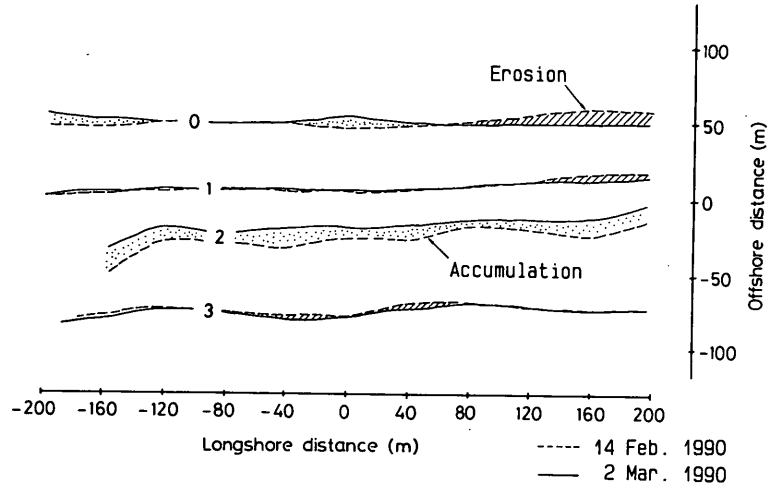

Fig.8(7) Foreshore topography change (Measurement C)

[Measurement D]

Figure 9(1) shows the significant wave heights and the significant wave periods. The significant wave heights rapidly increased from 0.5m to 2m on the 27th owing to a low atmospheric pressure. On the 30th, the heights started to decrease as the low pressure moved far away from the HORF. The significant wave periods were about 7s owing to wind waves.

Figure 9(2) shows the wave breaking positions and breaker types. Waves broke offshore from P210m during the days from June 27th to the 30th and from July 5th

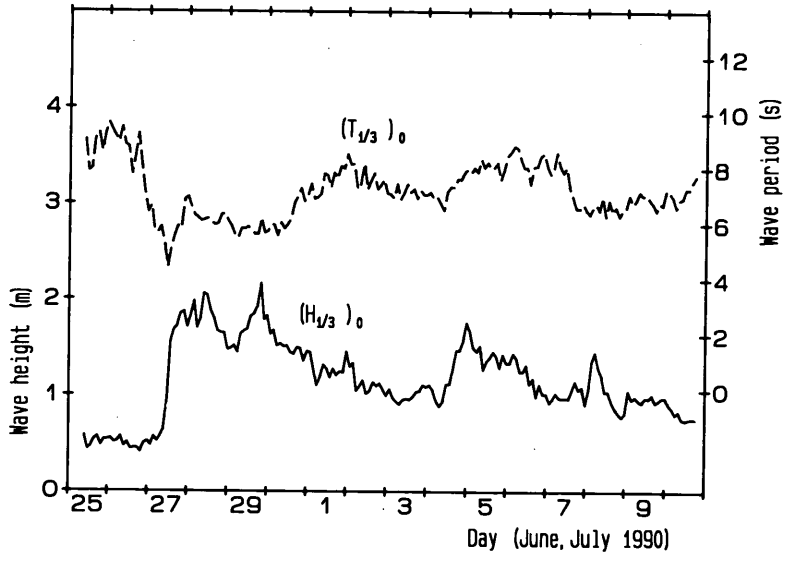

Fig.9(1) Offshore wave heights and wave periods (Measurement D)

to the 7th, when the wave heights were large. The predominant breaker type was spilling. From the 25th to the 27th, the primary breaking positions, which were in the region from P100m to P150m, varied considerably. From the 28th the wave breaking positions were almost fixed at P180m. The predominant breaker type was plunging. The wave breaking positions near the shoreline gradually moved seaward. The breaker type near the shoreline was plunging and spilling. The measurement station P145m was in the region a little shoreward of the breaking positions. Although the measurement station P80m was in the seaward region of the nearshore breaking positions until the 3rd, it was in the shoreward region of the positions since the 4th.

Figure 9(3) shows the levels of the electro-magnetic current meter, the tide and the bottom at the measurement station P145m, and Fig.9(4) shows those at P80m. The

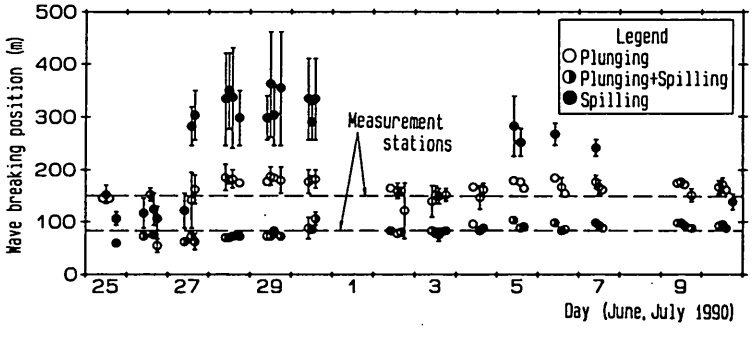

Fig.9(2) Wave breaking positions and breaker types (Measurement D)

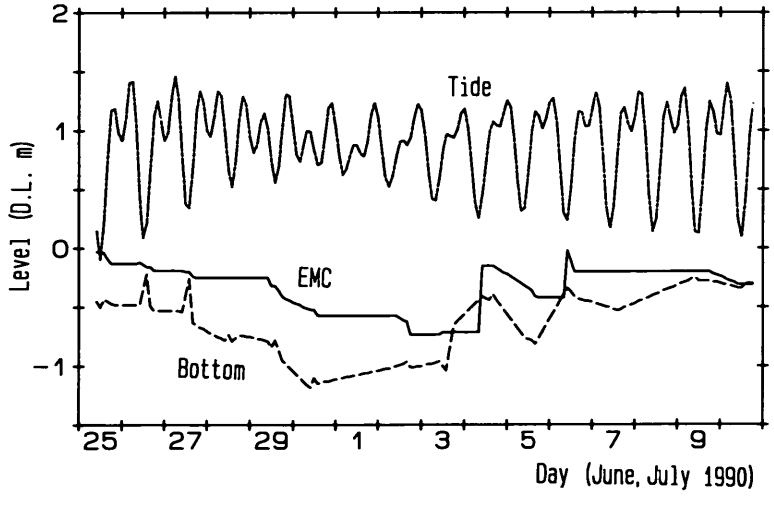

Fig.9(3) Levels of electro-magnetic current meter, tide and the bottom at P145m (Measurement D)

current meter at P80m was buried under the bottom from the 4th to the end of the series of measurements as shown in Fig.9(4). The current meter at P145m was occasionally buried.

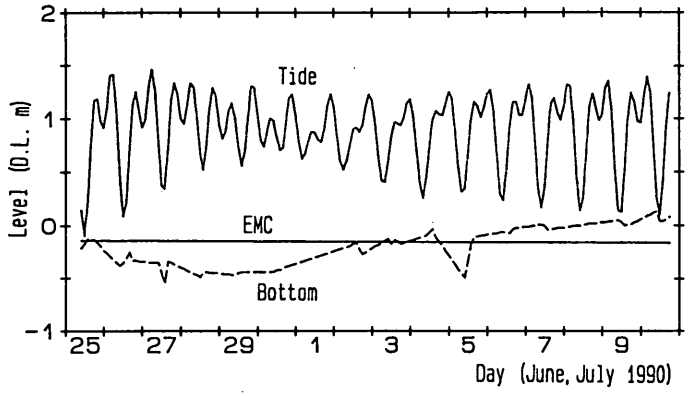

Fig.9(4) Levels of electro-magnetic current meter, tide and the bottom at P80m (Measurement D)

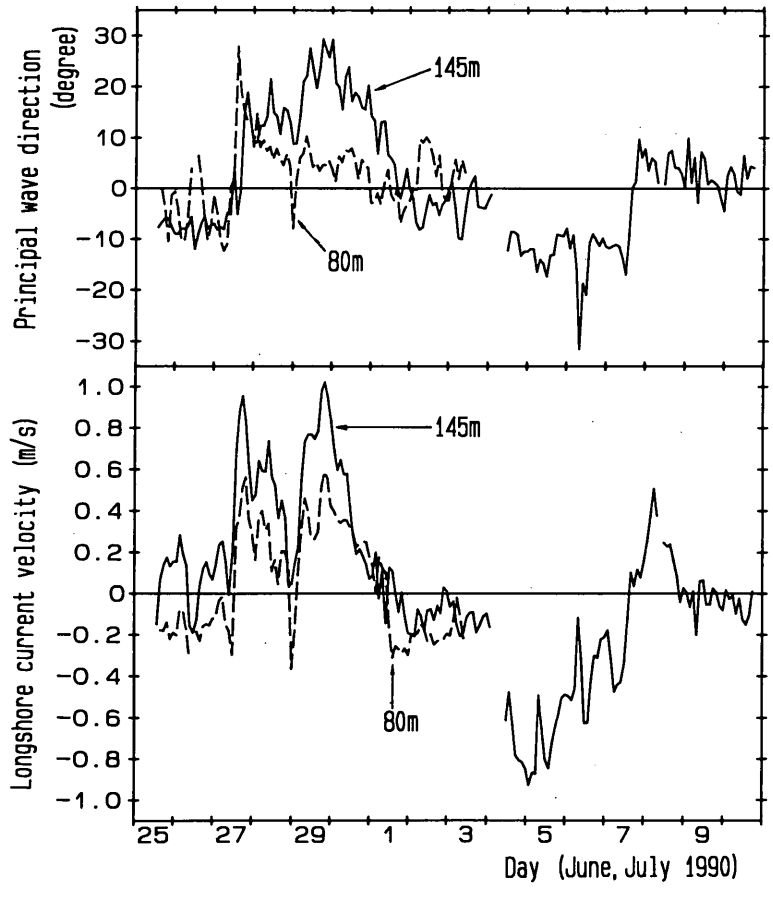

Fig.9(5) Principal wave directions and longshore current velocities (Measurement D)

The upper figure of Fig. 9(5) shows the principal wave directions, while the lower one shows the longshore current velocities. Although the principal wave directions at P145m changed from -30 degree to 30 degree, the absolute values of those at P80m were within 10 degree owing to wave refraction. The longshore velocities changed as the wave directions varied. The longshore velocities at P145m, which were larger than those at P80m, were sometimes more than 0.5m/s. A strong rip current did not occur near the HORF during the series of measurements.

Figure 9(6) shows the beach profile change. Accumulations and erosions occurred alternately. In the areas including the measurement stations P145m and P80m, sediments accumulated.

Figure 9(7) shows the change of the foreshore topography. Although the contour lines of D.L.0m, D.L.1m, and D.L.2m were sinuous alongshore, the amplitudes of the undulations were small.

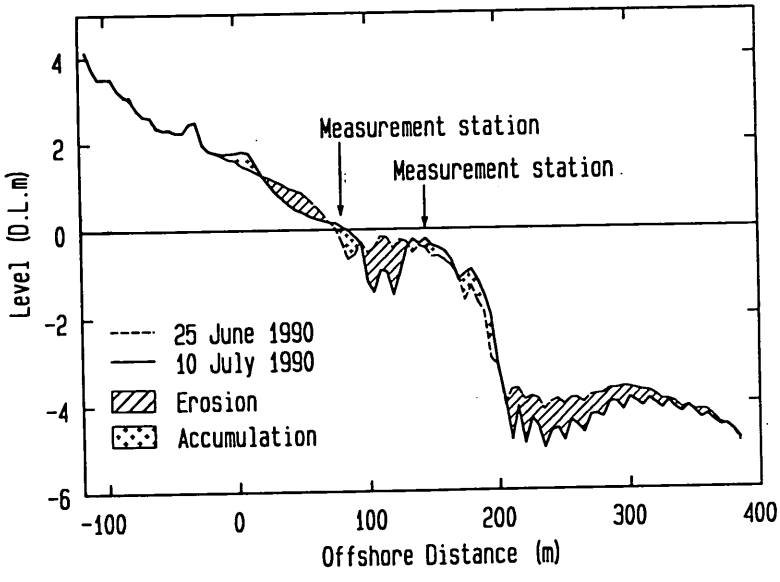

Fig.9(6) Beach profile change (Measurement D)

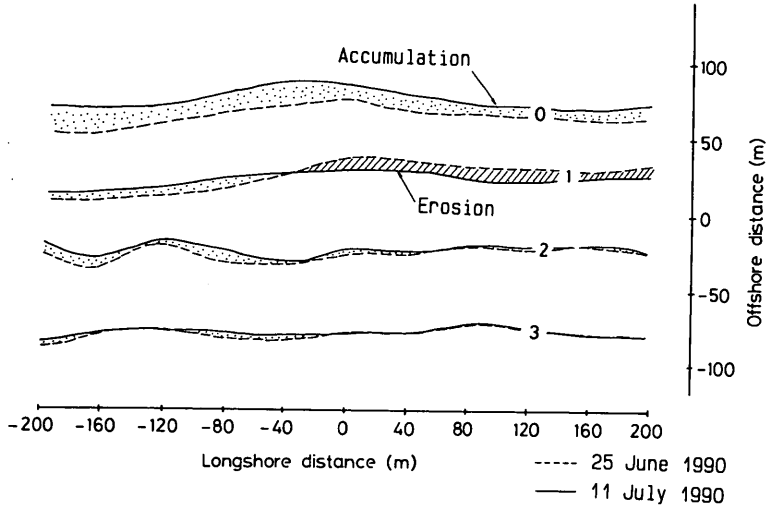

Fig.9(7) Foreshore topography change (Measurement D)

4. Relationships between cross-shore sediment transport rates and flow parameters

The relationships between cross-shore sediment transport rates and flow parameters have been already investigated in order to derive cross-shore sediment transport rate formulas. *Bowen* (1980), *Bailard* (1982) and *Stive* (1986) developed cross-shore sediment transport rate formulas considering nonlinear velocity properties based on Bagnold's energy concept (*Bagnold*, 1963). The suspended sediment transport is considered in their formulas, but the suspended sediment concentration is expressed by near-bottom velocities. This means that sediments are suspended by the turbulence originated at the bottom. Sediment suspensions due to the turbulence generated by wave breaking, which is dominant in the surf zone, is not taken into account in their formulas.

Dally and Dean (1984) proposed a cross-shore sediment transport rate formula in which time averaged cross-shore velocity and orbital velocity is used. They assumed that orbital velocity is sinusoidal and that sediments are suspended when a wave crest passes. Since the sediment suspensions can be considered to be caused by the upward and forward asymmetry of the velocity profile, in order to express the sand transport rate in the lower layer, parameters which represent nonlinear velocity properties are more suitable than those for sinusoidal velocities.

Katoh et al. (1985) proposed a local sediment transport rate formula based on the field data obtained with fluorescent sand tracers. They divided the advection speed of sand tracer into two components; one is that along the mean current direction and the other is that along the principal wave direction. The cross-shore component of this formula is expressed by Eq.(2).

$$Q=\frac{0.025}{g}\cdot(U_p)^2_{rms}\cdot\overline{v}-\frac{0.05}{g}(\sqrt{\beta_1})_{U_p}\cdot(U_p)^3_{rms}\cdot\cos\theta_p$$
$$+\frac{181}{g^4}\cdot sgn\left\{\left(\sqrt{\beta_1}\right)_{U_p}\right\}\cdot(U_p)^3_{rms}\cdot a^3\cdot\cos\theta_p, \qquad (2)$$

where $a=sgn(a_c)\cdot|a_c|^{1/3}, a_c=\frac{1}{N-1}\sum_{i=1}^{N-1}\left\{(\dot{U}_p)_i-(\overline{\dot{U}_p})\right\}^3$, Q is the

seaward sediment transport rate, U_p is the velocity along the principal wave direction, $(U_p)_{rms}$ is the root-mean-square value of $(U_p-\overline{U_p})$, g is the acceleration of gravity, and the overdot denotes the differentiation with respect to time. The value of $(\sqrt{\beta_1})_{U_p}$ is the skewness of the velocity along the principal wave direction and defined by Eq.(3).

$$(\sqrt{\beta_1})_{U_p} = -\left[\frac{1}{N}\sum_{i=1}^{N}\left\{(U_p)_i - \overline{U}_p\right\}^3 / (U_p)_{rms}^3\right] . \qquad (3)$$

Conventionally, velocity skewness is defined to be positive when the absolute values of the shoreward velocities are larger than those of seaward velocities, even though the velocity is defined to be positive in the seaward direction. Thus the signs of the second and third terms in Eq.(2) are opposite to those in the original paper by *Katoh et al.* (1985).

The coefficient of the right hand first term in Eq.(2) was determined on the basis of the sand tracer advection speed along the mean current direction; the first term represents the sum of the suspended load transport rate and the bed load transport rate due to time-averaged velocities.

The coefficients of the second and third terms in Eq.(2) were determined with the sand tracer advection speed along the principal wave direction. The second term indicates the cross-shore component of the bed sediment transport rate. *Katoh et al.* (1985) expressed the rate by using the third power of the velocity along the principal wave direction as did *Bowen* (1981) and *Bailard* (1982).

The third term in Eq.(2) represents the transport rate of the sediments suspended when a bore crest passes. *Katoh et al.* (1985) expressed the rate by taking into account the forward asymmetry of the velocity since they considered the shape of a bore is important for this transportation.

Goda (1985) has proposed a parameter which represents the forward asymmetry of wave profile. This parameter is referred to as atiltness and defined by Eq.(4). He utilized the property that the wave profile with forward asymmetry is changed into the upward asymmetric profile by differentiating with respect to time.

$$(\beta_3)_\eta = \frac{1}{N-1}\sum_{i=1}^{N-1}(\dot{\eta}_i - \overline{\dot{\eta}})^3 / \left\{\frac{1}{N-1}\sum_{i=1}^{N-1}(\dot{\eta}_i - \overline{\dot{\eta}})^2\right\}^{3/2} , \qquad (4)$$

where $(\beta_3)_\eta$ is the atiltness of wave profile.

Applying the concept to the velocity field, *Katoh et al.* (1985) used the third power of the fluid acceleration to represent the sediment transport rate due to the forward asymmetry of the velocity.

They assumed the sediment is transported seaward by incident waves. They considered, however, the sediment is transported shoreward when the infragravity waves develop since the duration time of the shoreward velocity is larger than that of the seaward velocity. Although the velocity skewness in the surf zone is usually shoreward, it is seaward when infragravity waves develop. Consequently, they expressed the direction of this transportation by the sign of the velocity skewness.

The daily sediment transport rates calculated by Eq.(2) are compared with the measured ones in Fig.10. The calculated sediment transport rate is the sum of the twelve transport rates in two hours. The rate in two hours is estimated using Eq.(2) with the parameters calculated with the twenty minutes sample, which is obtained every two hours. The parameters are assumed to be the representative values in two hours. When the current

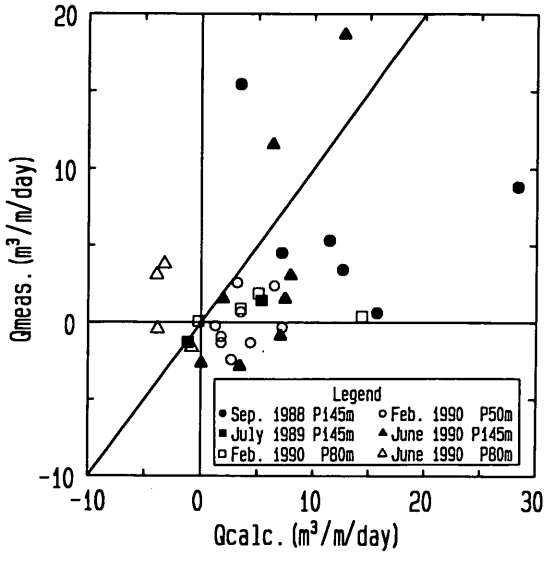

Fig.10 Comparison of the measured seaward sediment transport rate with the value predicted by Eq.(2) derived on the basis of the result by *Katoh et al.* (1985)

meter was out of sea water at P50m or P80m and the velocities could not be measured, the rate is assumed to have been zero.

The measured rate of cross-shore sediment transport is the volume difference in the region from the measurement station to P-115m, where no net sediment transport occurs. In this evaluation, it is assumed that the longshore sediment transport did not affect the beach profile change. This assumption is supported by the fact that the topography changes on the foreshore were two dimensional as shown in Figs. 6(7), 7(6), 8(7) and 9(7). While the measurement stations P50m and P80m are included in these figures, the measurement station P145m is not included. The bottom topography near P145m, however, can be analogized from the foreshore topography since the foreshore one is related to the offshore one. The longshore undulations in the foreshore topographies were small except for those on July 19th in 1989. Consequently, it can be assumed that the effect of longshore sediment transport to the beach profile change was small. As to the foreshore topography on July 19th in 1989, a remarkable longshore undulation is noticed in the contour line of D.L.0m. The HORF, however, was located around the middle of the most regressed and advanced positions. It means that the beach profile along the HORF was an averaged one in the longshore variation. Consequently, it is considered that the longshore sediment transport gave little effect on the change of the beach profile along the HORF for the day of July 19th in 1989.

As shown in Fig.10, the calculated seaward sediment transport rates are larger than the measured ones. Although the coefficient of the right hand first term in Eq.(2) was determined with the mean current velocity, the coefficient of the first term for the cross-shore current velocity is probably different from that for the longshore current velocity owing to the fluid oscillatory motion. This difference may be a principal reason why the calculated rates are larger than the measured values.

Moreover, the mechanism of suspended load transport expressed by the first term and that expressed by the third term are indistinguishable. Therefore by the consideration of three independent mechanisms of cross-shore sand transport as shown with the symbols Ⓐ, Ⓑ and Ⓒ in Fig.11 and by the examination of the contribution rates of the mechanisms

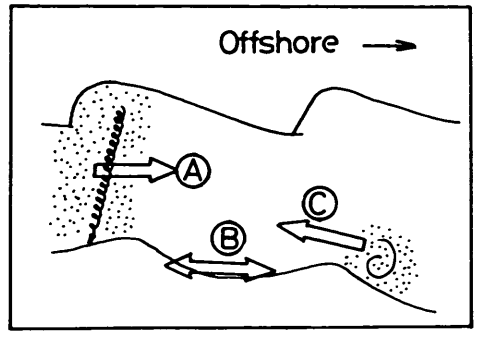

Fig.11 Definition sketch of sand movements considered in Eq.(5)

to the cross-shore sediment transport rates, the relationship between the cross-shore sediment transport rates and the flow parameters is investigated.

A new relationship is assumed to be given by Eq.(5).

$$Q = c_1 h\overline{v}\left(\frac{\eta_{rms}}{w_o T}\right)^{c_2}\left(\frac{\eta_{rms}}{h}\right)^{c_3} + c_4\frac{\cos\theta_p}{g}\overline{\left\{U_p - \overline{U}_p\right) + c_5\overline{U}_p\right\}^3} + c_6\cos\theta_p\left\{\frac{(U_p)^3_{rms}}{g}\right\}\left(\frac{a}{g}\right)^{c_7}, \quad (5)$$

where h is the water depth, $\overline{v}$ is the time mean seaward velocity, η_{rms} is the root-mean-square value of $(\eta-\overline{\eta})$, η is the water surface elevation, w_o is the fall velocity of sediment in sea water, and T is the wave period. In this paper, the offshore significant wave period is used as the value of T.

The right hand first term in Eq.(5) corresponds to the sand transport in type Ⓐ. This is the transport of the sediment suspended by the turbulence due to wave breaking. Judging from the observation result by *Nadaoka et al.* (1988), the sediment is considered to be suspended up to the water surface and fall down to the bottom after the time of several waves. Hence the transport rate can be expressed as a product of the water depth, the time-averaged cross-shore velocity and the suspended sediment concentration.

Kana (1978) has reported that the suspended sediment concentration increases as the wave height-water depth ratio increases. The ratio is considered to express the strength of the turbulence on the bottom, which is generated by wave breaking; the rate of the sediments suspended by the turbulence is assumed to be a function of the ratio.

The value of η_{rms}/w_oT, which is one fourth of the Dean's number, is also used for the representation of the suspended sediment concentration. The value of η_{rms} expresses the strength of the turbulence in the middle layer which keeps the sediments in suspension. Moreover, the value of η_{rms} is proportional to the suspension height because the value of η_{rms} is nearly one fourth of the significant wave height; in the surf zone, the wave height is almost proportional to the water depth, which is equal to the suspension height. When the wave period is assumed to be related to the suspension interval, the value of w_oT expresses the falling distance of the sediment between the successive sediment suspensions. Thus the value of η_{rms}/w_oT is considered to express the residual rate of the suspended sediments. Accordingly, the concentration is represented with the wave height-water depth ratio and the value of η_{rms}/w_oT.

In the second term in Eq.(5), the transport rate of the sediment moving on the

bottom, shown in type Ⓑ, is expressed with the third power of the velocity near the bottom as *Bowen* (1981), *Bailard* (1981) and *Katoh et al.* (1985). The velocity near the bottom can be represented by the sum of the time-averaged velocity and the orbital velocity. The orbital velocity measured in the middle layer is used as the orbital velocity near the bottom on the basis of the long waves approximation. On the other hand, the estimation of the time-averaged velocity near the bottom is not established; the velocity is assumed to be proportional to the time-averaged value of the velocities measured in the middle layer.

The transport of the sediment suspended in the vicinity of ripples, which is shown in type Ⓒ, is expressed by the right hand third term in Eq.(5). *Sunamura* (1980) have reported that a sediment moves seaward over asymmetric ripples in a wave flume. However, *Bijker et al.* (1976) has showed that the sediment transport rate over ripples was shoreward at the point where the shoreward acceleration is greater than the seaward one. *Irie and Nadaoka* (1984) have also reported that the sediment particles moved shoreward under standing waves in the vicinity of ripples where the shoreward acceleration is larger than the seaward one. Accordingly, the sediment transport rate over ripples is expressed with the fluid acceleration in the third term.

When there are no ripples in the surf zone, the coefficient C_6, which is determined on the basis of the field data with statistical method, is close to zero.

The sand transport rate at a measurement station is assumed to be evaluated only with the hydraulic properties at the station. Outside the surf zone, however, the assumption can not be adopted. The reason is that the suspended sediment concentration at a station just outside the surf zone is greater than that predicted with the hydraulic properties at the station since the water with much sand is moved to the station from the surf zone by return flows. Thus the data outside the surf zone are not used in this chapter.

Besides that, the two types of data mentioned below are eliminated since the phenomena at the measurement station are no longer two dimensional.

a. The data obtained near a rip current,
b. The data obtained when the sea bottom change is considered to be three dimensional.

On the basis of the velocity data and the measured sand transport rates in the surf zone, the seven coefficients in Eq.(5) are evaluated with the Powell method in nonlinear programing. The determined coefficients are listed in Table 5. The maximum sand transport rate calculated by the second term in Eq.(5) is 0.03 $m^3/m/day$. Since it is approximately 0.001 times as much as those calculated by the other

Table 5 Values of coefficients in Eq.(5)

C_1	1.10×10^{-4}
C_2	3.59
C_3	0.742
C_4	2.98×10^{-7}
C_5	25.4
C_6	0.447
C_7	1.54

terms, the second term is omitted. Accordingly, the new relationship between the cross-shore sediment transport rates and the flow parameters is expressed by Eq.(6).

$$Q = 1.10\times10^{-4}\cdot h\cdot\bar{v}\cdot\left(\frac{\eta_{rms}}{w_o T}\right)^{3.59}\cdot\left(\frac{\eta_{rms}}{h}\right)^{0.742}$$
$$+0.447\cos\theta_p\cdot\left\{\frac{(U_p)^3_{rms}}{g}\right\}\cdot\left(\frac{a}{g}\right)^{1.54} \qquad (6)$$

Equation (6) shows that time-averaged cross-shore velocities are important for the seaward sediment transport in the surf zone. Since the coefficient C6 in the right hand third term in Eq.(5) is not zero, ripples or bottom undulations are considered to exist even in the surf zone and have an important role for the shoreward cross-shore sediment transport. The second term in Eq.(5), which is related to the velocity skewness, was eliminated as mentioned before. This elimination indicates that the suspended load, includes the sediment moving in the vicinity of ripples, was predominant than bed load in the surf zone during the series of measurements.

The sand transport rates calculated by Eq.(6) are compared with the measured ones in Fig.12. Most of the calculated values agree with the measured values near the wave breaking positions as well as those in the middle of the surf zone. Therefore it is concluded that the new relationship between the cross-shore sediment transport rates and flow parameters, which is expressed by Eq.(6), is valid extensively in the surf zone. However, several calculated values are different from the measured values. Thus the causes of the differences are investigated.

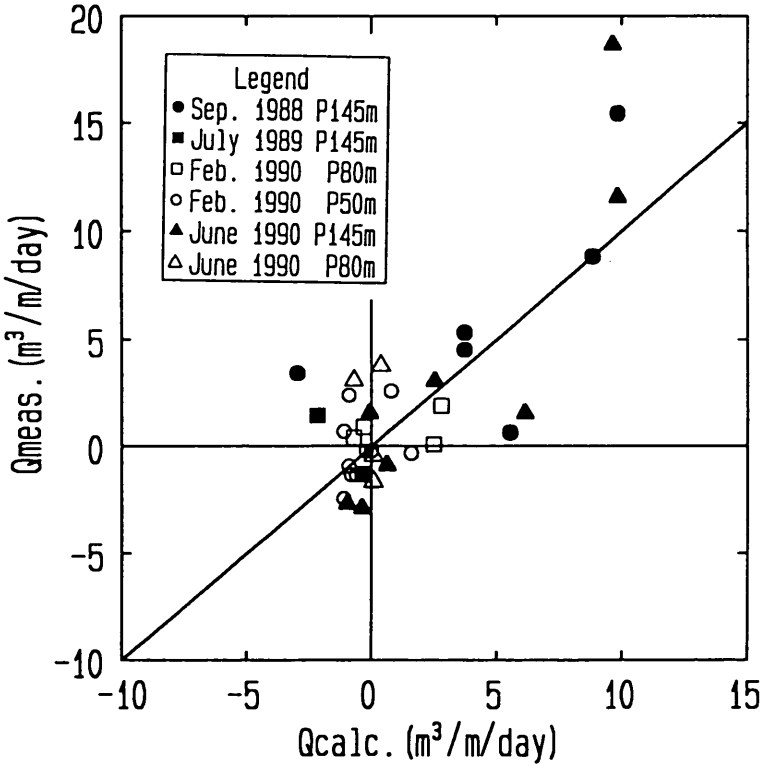

Fig.12 Comparison of the measured seaward sediment transport rate with the value predicted by Eq.(6)

The calculated seaward sediment transport rates during the periods ①, ② and ③ at P80m or P50m are smaller than the measured ones as shown in Fig.13. The measurement stations P80m and P50m were located near the foreshore. The foreshore was eroded during each period as shown in Figures 14 (1), (2) and (3). The cause

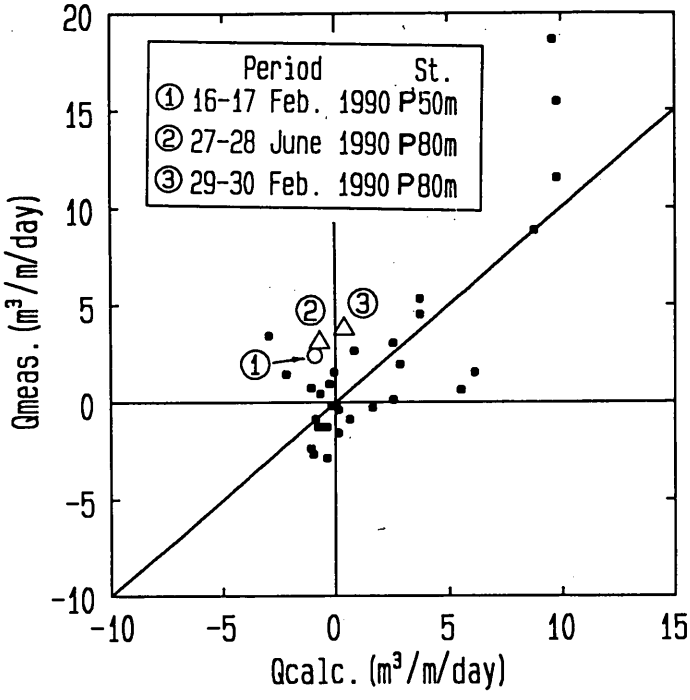

Fig.13 The seaward sediment transport rates during the periods ①, ②, and ③

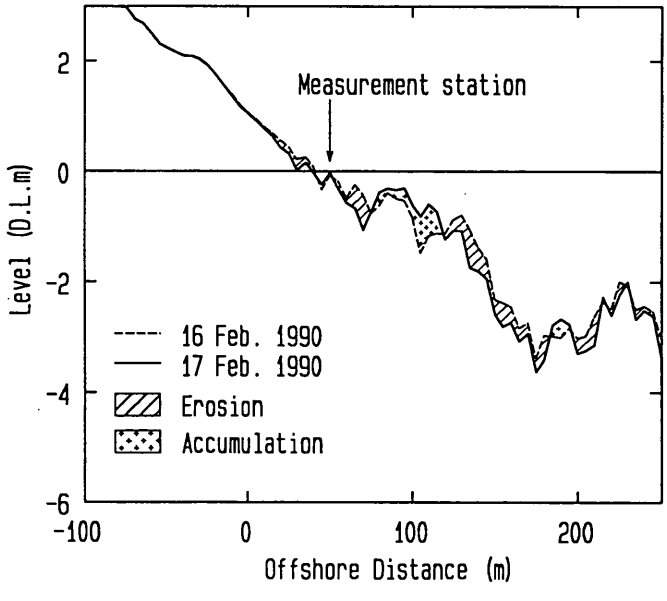

Fig.14(1) Beach profile change from the 16th to the 17th of February, 1990

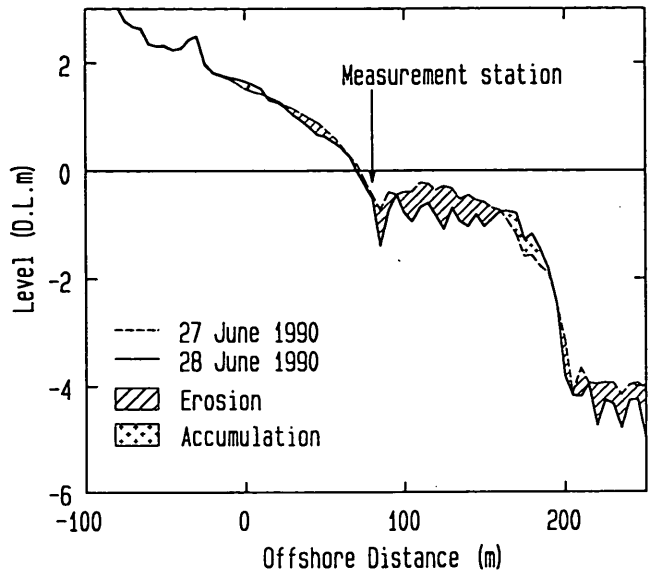

Fig.14(2) Beach profile change from the 27th to the 28th of June, 1990

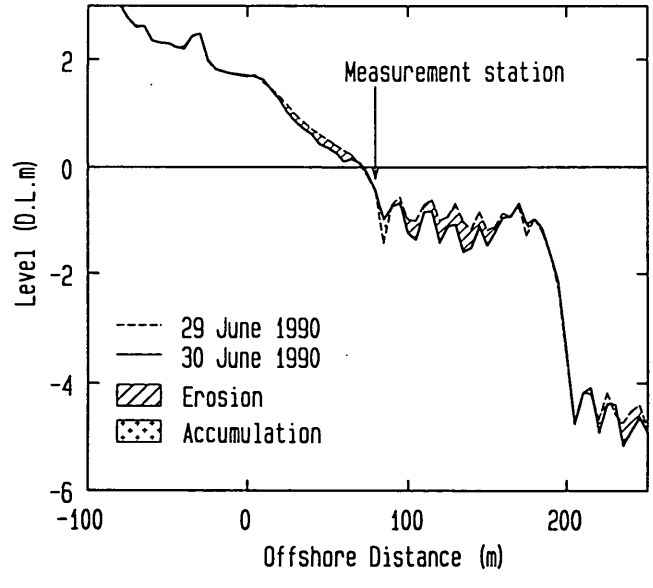

Fig.14(3) Beach profile change from the 29th to the 30th of February, 1990

of the differences between the calculated values and the measured values is considered to be that the foreshore erosion occurs through another mechanism of sand transport, which is different from the two mechanisms considered in Eq.(6).

Figure 15 shows that the calculated values during the periods ④ and ⑤ at P145m agree with measured ones. However, the calculated values during the periods ⑥ and ⑦ differ from the measured values. Figures 16 (1) to (4) show the beach profile

changes during these periods. The properties of beach profile changes during the periods ④ and ⑤ are as follows:

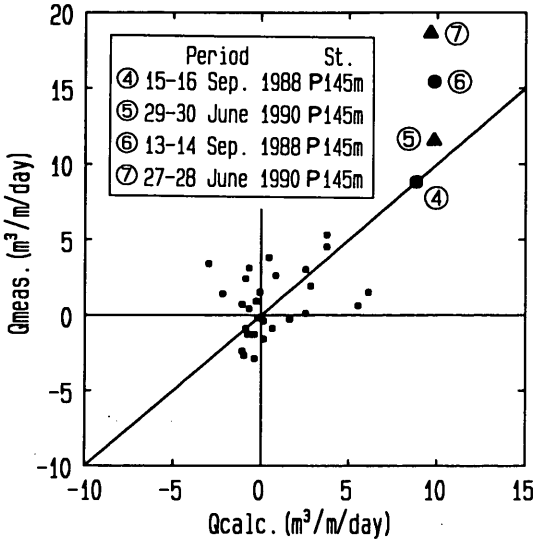

Fig.15 The seaward sediment transport rates during the periods ④, ⑤, ⑥, and ⑦

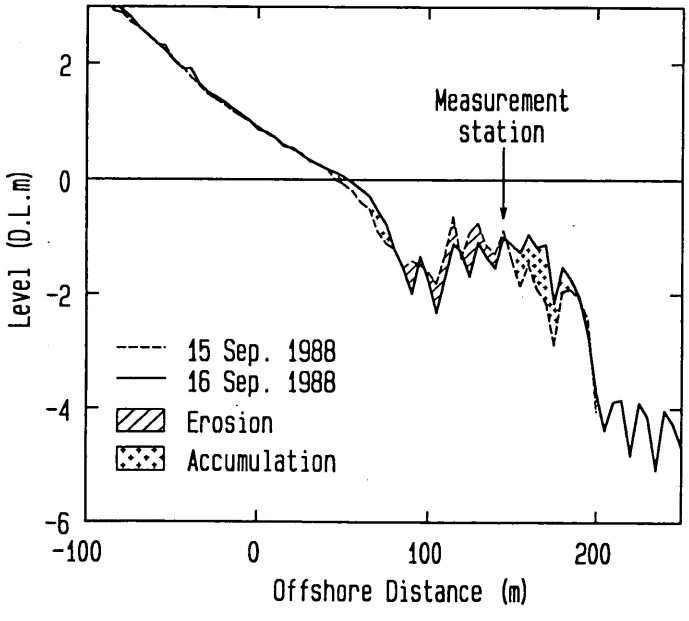

Fig.16(1) Beach profile change from the 15th to the 16th of September, 1988

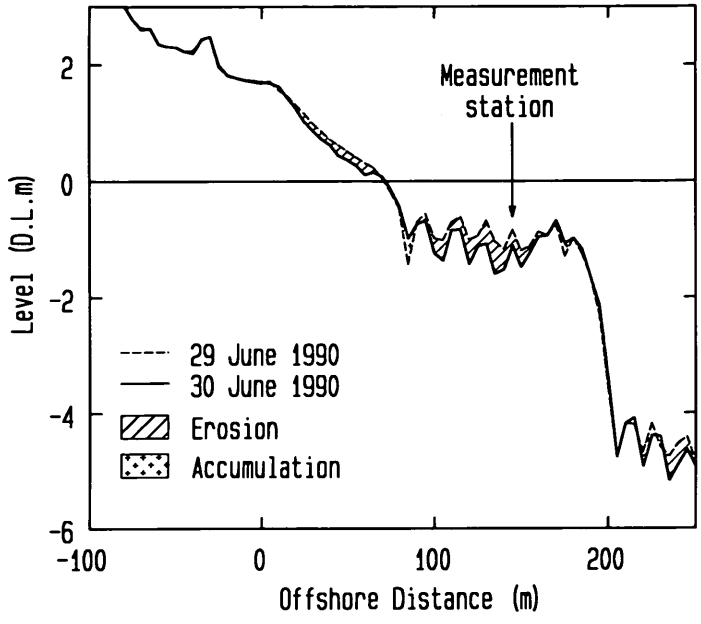

Fig.16(2) Beach profile change from the 29th to the 30th of June, 1990

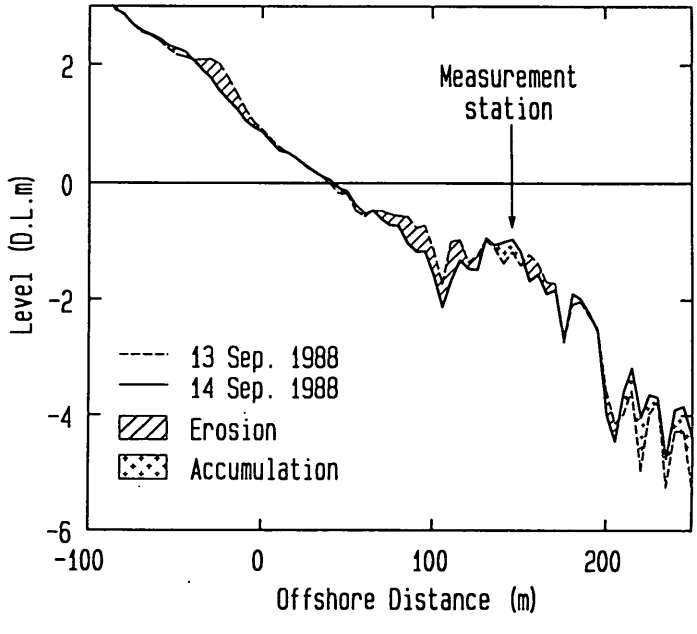

Fig.16(3) Beach profile change from the 13th to the 14th of September, 1988

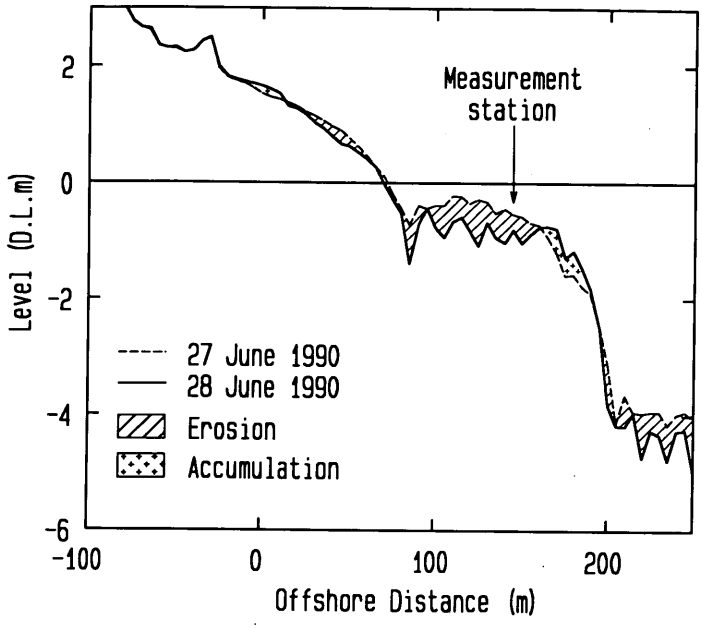

Fig.16(4) Beach profile change from the 27th to the 28th of June, 1990

1. The foreshore was not eroded during the period ④ as shown in Fig.16 (1).
2. The foreshore was eroded during the period ⑤ as shown in Fig.16 (2). Sediments which had been in the foreshore, however, accumulated in the region from P70m to P90m.

On the other hand, during the periods ⑥ and ⑦, the foreshore was eroded, and there were no accumulation areas between the foreshore and the measurement station. The two characteristics represent that the sediment which had been in the foreshore before the erosion passed through the measurement station during the periods. Thus it is concluded that a cross-shore sediment transport rate in the surf zone can be calculated with the flow parameters by Eq.(6) when the foreshore profile change do not affect the rate. However, the transport rate cannot be calculated by Eq.(6) when the rate is affected by the foreshore profile change.

The calculated seaward transport rate during the period ⑧ is smaller than the measured one as shown in Fig.17. The foreshore was not eroded during the period (Fig.18). As mentioned in **3.4**, a rip current was observed near the HORF during the period ⑧, at eight thirty on September 20th in 1988, while no other rip currents were observed near the HORF on 20th. When a rip current exists, the phenomena near the rip current are three dimensional; the cross-shore sediment transport rate can not be evaluated by Eq.(6). The cause of the difference between the calculated value and the measured value during period ⑧ may be the rip current.

The calculated seaward sediment transport rates during the periods ⑨ and ⑩ are larger than the measured ones as shown in Fig.19. Figures 20 (1) and (2) show that the beach profile changes during the periods were small. The small sand transport rates occurred at the day after when the beach was eroded more heavily in the field than in the calculation, as the arrows indicate in Fig.19. Since the beach profile may have reached to the equilibrium one for one day, the beach profile changes at the next day may have been small.

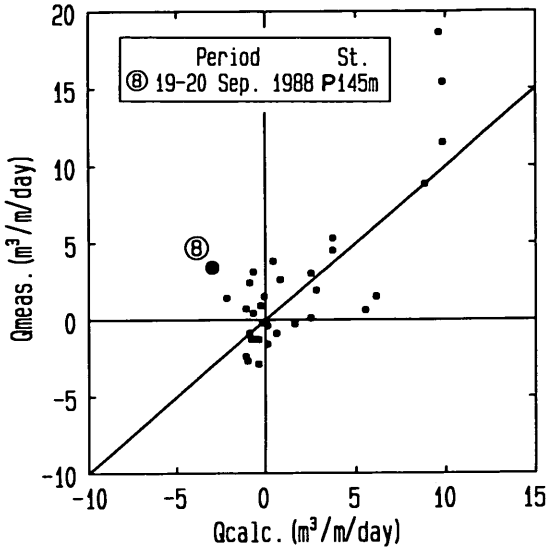

Fig.17 The seaward sediment transport rate during the period ⑧

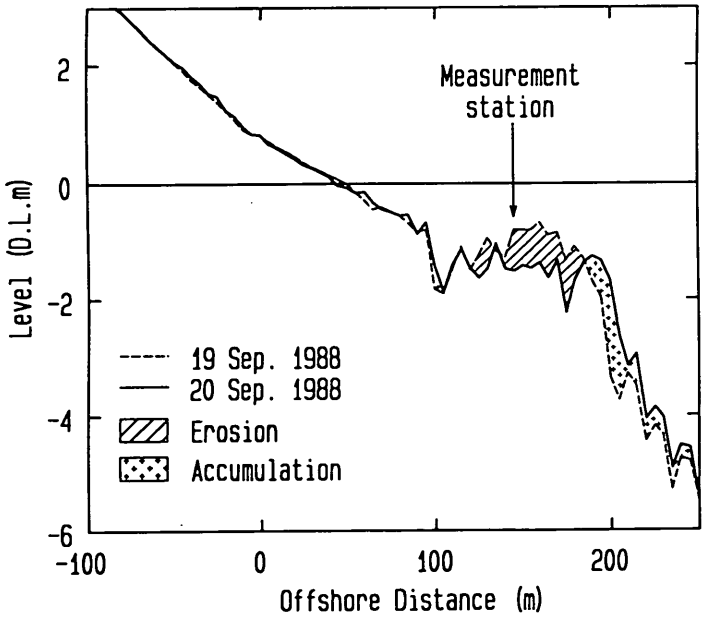

Fig.18 Beach profile change from the 19th to the 20th of September, 1988

The new relationship between the cross-shore sediment transport rates and the flow parameters, which is expressed by Eq.(6), was estimated with the field data including those during periods ① to ③ and periods ⑥ to ⑩, which are considered to be out of the range for Eq.(6). Hence the coefficients of Eq.(5) should be reevaluated without the unsuitable data such as those when the erosion volume in the foreshore was relatively large. The coefficients, however, are not reevaluated since there is no standard for judging whether the erosion volume is small enough to be used for the evaluation of the coefficients in Eq.(5) or not.

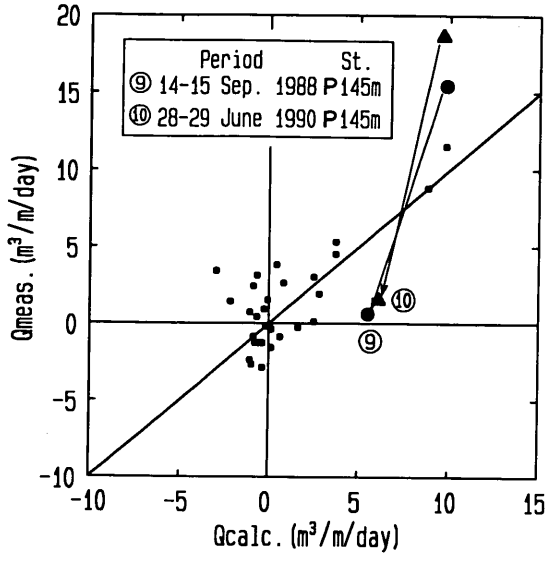

Fig.19 The seaward sediment transport rates during the periods ⑨ and ⑩

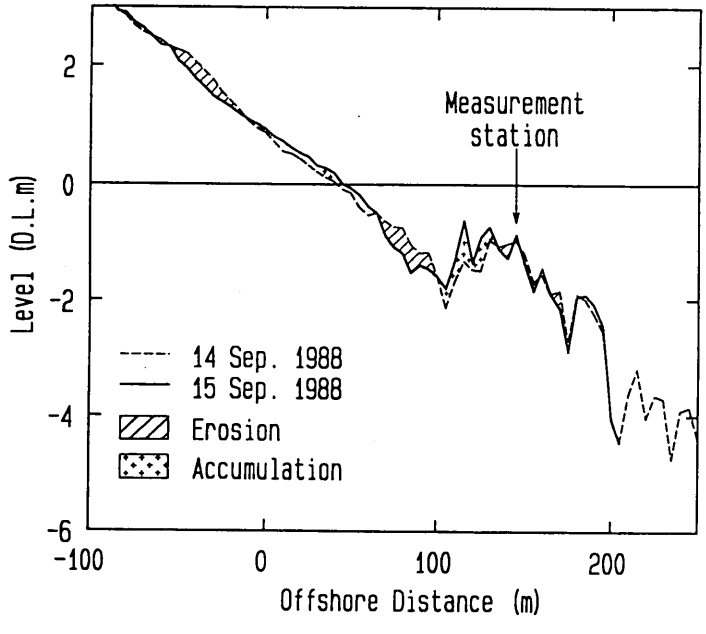

Fig.20(1) Beach profile change from the 14th to the 15th of September, 1988

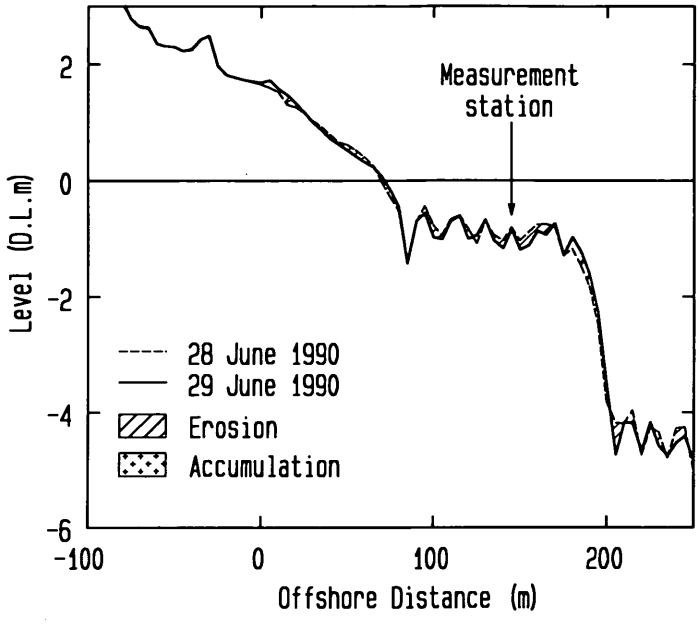

Fig.20(2) Beach profile change from the 28th to the 29th of June, 1990

5. Relationships between flow parameters and wave parameters

The time-averaged cross-shore velocity, the orbital velocity and the forward asymmetry of velocity profile are strongly related to the cross-shore sediment transport rate. However, it is difficult to evaluate the flow parameters by the direct measurements of current velocities. The wave parameters such as the wave height and the wave period can be predicted with the offshore wave parameters using various wave transformation models. If the flow parameters can be predicted with the wave parameters, one can easily evaluate the flow parameters. Therefore the relationships between various flow parameters and the wave parameters are investigated in this chapter.

5.1 Time-averaged cross-shore velocities

The time series of the time-averaged cross-shore velocities for twenty minutes are shown in Figs. 21(1) to (4), in which seaward velocities are defined to be positive.

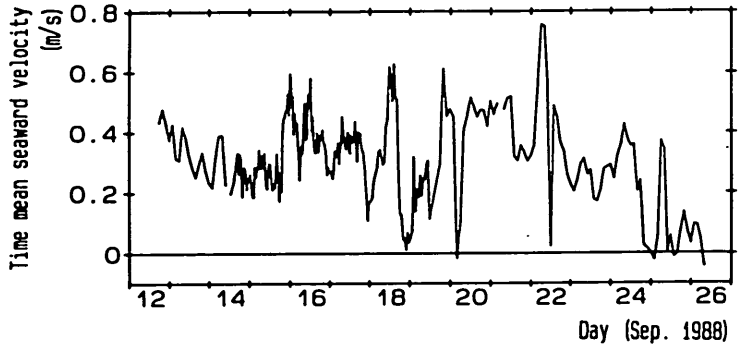

Fig.21(1) Time series of time-averaged seaward velocities measured during Measurement A

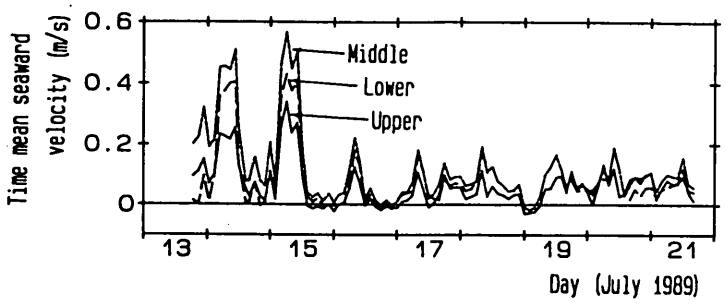

Fig.21(2) Time series of time-averaged seaward velocities measured during Measurement B

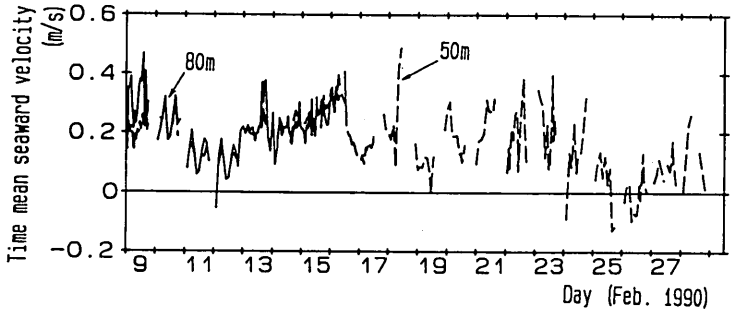

Fig.21(3) Time series of time-averaged seaward velocities measured during Measurement C

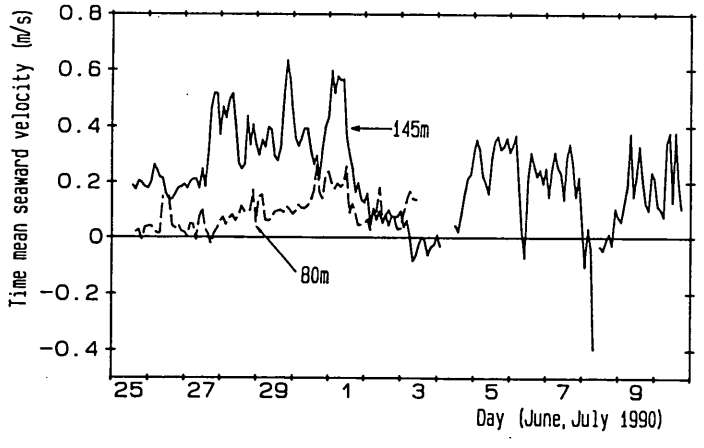

Fig.21(4) Time series of time-averaged seaward velocities measured during Measurement D

Almost all of the time-averaged cross-shore velocities are seaward because of return flows or undertows, which compensate the shoreward mass flux above wave trough levels.

Svendsen (1984) has theoretically obtained the solution for the depth mean value of time-averaged cross-shore velocity below a wave trough level in the surf zone.

He assumed that the cross-shore velocity in a surface roller, which is a shoreward progressing bore generated by wave breaking, is equal to the wave celerity. Equation (7) represents his result.

$$\overline{v} = C\frac{H^2}{h^2}(B_o + A\cdot\frac{h}{L}), \qquad (7)$$

where $B_o = \frac{1}{H^2}\cdot\frac{1}{T}\int_0^T(\eta-\overline{\eta})^2 dt$, C is the wave celerity, H is the wave height, A is the surface roller area parameter, and L is the wavelength.

The time-averaged velocity consists of two components. The right hand first term in Eq.(7) is the velocity due to water surface variations. The right hand second term in Eq.(7) is the velocity due to the turbulence generated by wave breaking; this term is valid only in the surf zone.

Equation (7) has been derived for regular waves. The right hand first term can be changed into equation (8) in order to apply it for irregular waves.

$$\overline{v}_{wave} = C\eta_{rms}^2 / h^2, \qquad (8)$$

where $\overline{v}_{wave}$ is the time mean cross-shore velocity due to water surface variations.

Figure 22 shows the comparison of the time-averaged cross-shore velocities predicted by Eq.(8) with the values measured outside the surf zone during Measurement B (July in 1989). The solid line expresses the predicted values, and the circles, tetragons and triangles express the measured values. Since the predicted velocities are almost equal to the measured values except for several values, it is confirmed that Eq.(8) can be used for the time-averaged cross-shore velocity generated by the periodical water surface variations.

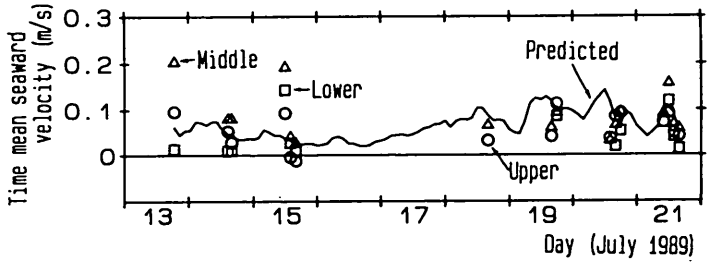

Fig.22 Comparison between the predicted velocities due to the periodical surface variations and time-averaged values of the velocities measured outside the surf zone during Measurement B

The right hand second term in Eq.(7) is applied when all waves are broken. While all periodic waves are broken in the surf zone, all random waves are not broken even in the surf zone since the wave breaking positions vary. In order to apply the second term to irregular waves field, the value of P_b, which is the fraction of all breaking waves, is introduced as *Stive and Battjes* (1984). The value is added to the second term, and Eq.(9) is finally obtained as the theoretical result of the time-averaged cross-shore velocity.

$$\overline{v} = \frac{C\eta_{rms}^2}{h^2} + P_b \cdot A \cdot \frac{H^2}{hT} \quad . \qquad (9)$$

Concerning the right hand second term in Eq.(9), *Svendsen* (1984) has used 0.9 as the value of parameter A based on the Duncan's experimental data for the breaking waves behind a hydrofoil. *Okayasu et al.* (1988) has placed 2.3 as the value of A based on their laboratory data. The two values used as the parameter A are different. In order to investigate the property of the value of A, it is calculated with the time-averaged cross-shore velocities by Eq.(10), which is the rewritten form of Eq.(9).

$$A = (\overline{v} - \frac{C\eta_{rms}^2}{h^2}) / (\frac{P_b \cdot H^2}{h \cdot T}) \quad . \qquad (10)$$

The error in parameter A calculated by Eq.(10) is mainly caused by the errors in three factors, which are the time-averaged cross-shore velocity $\overline{v}$, the fraction of breaking waves, P_b and the water depth, h. The errors in parameter A due to the errors in the three factors can be estimated by Eqs. (11), (12), and (13), which are the products of the errors in the factors and the change of the parameter A with the factors.

$$(E_A)_{\overline{v}} = \frac{\partial A}{\partial \overline{v}} \cdot E_{\overline{v}}, \qquad (11)$$

$$(E_A)_{P_b} = \frac{\partial A}{\partial P_b} \cdot E_{P_b}, \qquad (12)$$

$$(E_A)_h = \frac{\partial A}{\partial h} \cdot E_h, \qquad (13)$$

where $(E_A)_{\overline{v}}$, $(E_A)_{P_b}$ and $(E_A)_h$ are the errors in parameter A due to the errors in $\overline{v}$, P_b and h, and E_v, E_{p_b} and E_h are the errors in $\overline{v}$, P_b and h.

The error included in the time-averaged velocity is due to two causes. One is the offset drift of the electro-magnetic current meter mentioned before. The value of 0.01m/s is assumed as the error caused by the drift since the drifts of the electro-magnetic current meters except for EMC A were within 0.02m/s as shown in Table 4. The other is a nearshore current system, which includes rip currents. The phenomena near rip currents are no longer two dimensional while Eq.(9) is for a two dimensional phenomenon. On the other hand, the phenomena far from a rip current are nearly two dimensional. However, a rip current affects the cross-shore velocities even at the point far from the rip current. Since a certain volume of the water outside a rip current flows into the rip current for compensating the water volume transported seaward within the current, the seaward cross-shore current velocities at the points far from the rip current are smaller than those in two dimensional return flows. One can approximately estimate the difference between the velocity affected by a rip current and that in two dimensional return flow by dividing the seaward water volume within a rip current with the sectional area between the adjacent rip currents. The rip current spacing is about three times as wide as a surf zone width in average (*Sasaki and Horikawa*, 1975). Since the mean width of the surf zone during the measurements is 150m, the rip current spacing is evaluated to be 450m. When the width and the velocity of the rip current are assumed to be 20m and 1m/s, the seaward water volume

within the rip current becomes $20h_b$ (m^3/s), where h_b expresses the water depth at wave breaking position. The sectional area between the adjacent rip currents is $450h_b$ m^2; the error caused by the rip current is estimated to be 0.04m/s ($=20h_b/450h_b$). Consequently, the error included in the time-averaged cross-shore velocity is 0.05m/s, which is the sum of the error caused by a offset drift and that by a rip current.

The velocity measured with one current meter is not the depth averaged velocity. However, the error due to the vertical distributions of time-averaged cross-shore velocities is not considered since one can assume that time-averaged cross-shore velocities are vertically constant in the middle layer in the surf zone judging from the results by *Nadaoka and Kondoh* (1982).

When the errors included in the fraction of breaking waves and the water depth are assumed to be 0.1 and 0.05m, the sum of the errors in parameter A due to the errors in the three factors is concentrated in the range from 0.5 to 2.0.

In the investigation of parameter A, the datum including a large total error, which is presumed to be larger than 5.0, is eliminated. Besides that, the two types of data mentioned below are omitted as in **4.** since the phenomena at the measurement station are no longer two dimensional.

a. The data obtained near a rip current,
b. The data obtained when a sea bottom change is considered to be three dimensional.

Figures 23 (1),(2) and (3) show the variations of the values of A calculated from Eq.(10). The value of $4\eta_{rms}$ and the offshore significant wave period are substituted into H and T. The solid lines extending from circles express the total errors evaluated using Eq.(11), (12) and (13). The values of A are no longer constant. They vary from -3.5 to 10.

The relationship between the value of A and the distance from the wave breaking position to the measurement station is investigated. Figs.24 (1) and (2) show the relationships among the data obtained when the ratios of the plunging breakers to all breakers, R_p, are 0.7 and 0.8, respectively. The ordinates indicate the relative distances, R_d, which are the nondimensionalized distances between the measurement stations and the shorelines divided with the surf zone widths. The value of A decreases as R_d decreases in both cases. *Nadaoka and Kondoh* (1982) reported that the turbulence in a bore decays

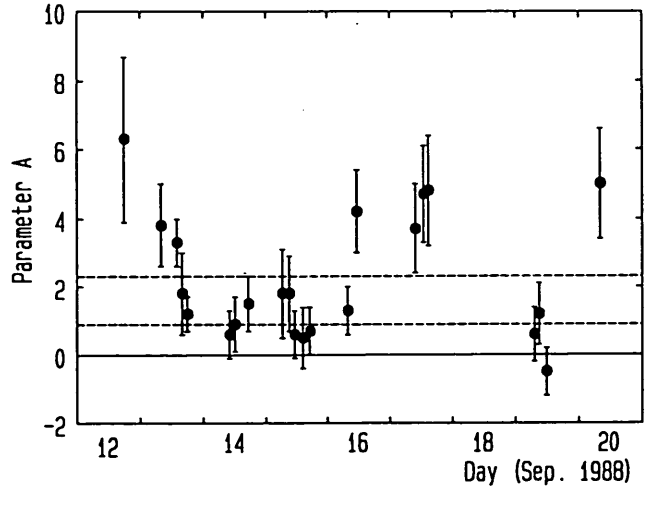

Fig.23(1) Variations of the parameter A (Measurement A)

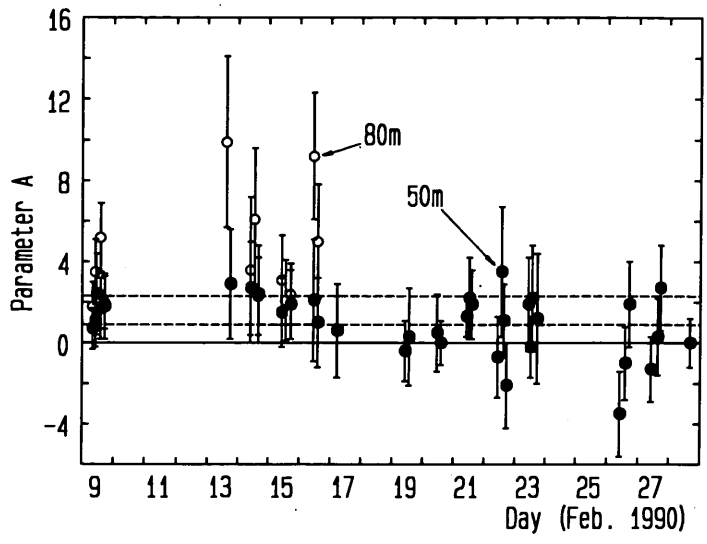

Fig.23(2) Variations of the parameter *A* (Measurement C)

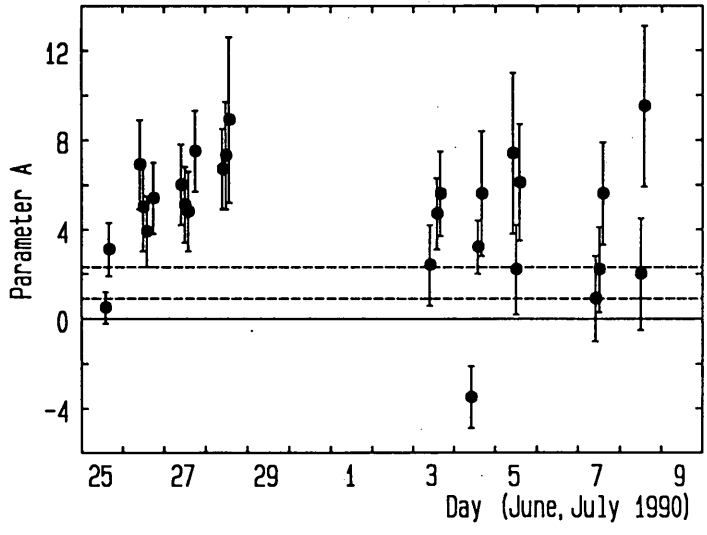

Fig.23(3) Variations of the parameter *A* (Measurement D)

as the bore propagates in the surf zone. As a result, the time-averaged velocity due to the turbulence decreases. Hence the value of *A* decreases as the distance from the breaking position increases.

The value of *A* is plotted against the plunging breaker ratio in Figs.25 (1) and (2). The figures show the relationships among the data obtained where the relative distances are from 0.6 to 0.8, and from 0.8 to 1.0. The marks "X", which are connected by a solid line, represent the averages among the data whose plunging breaker ratios

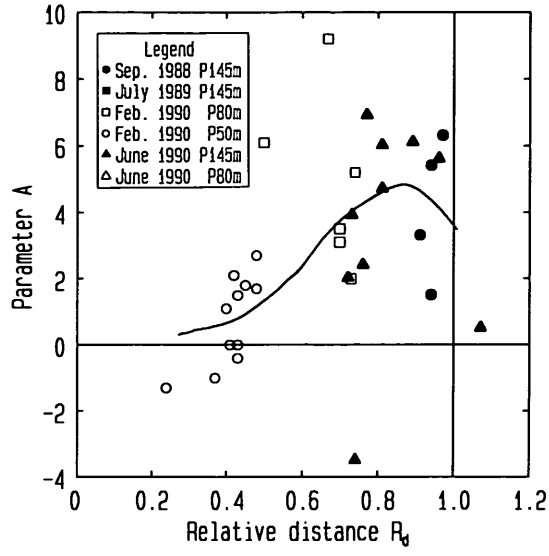

Fig.24(1) The relationship between the relative distance and the parameter A when R_P is 0.7

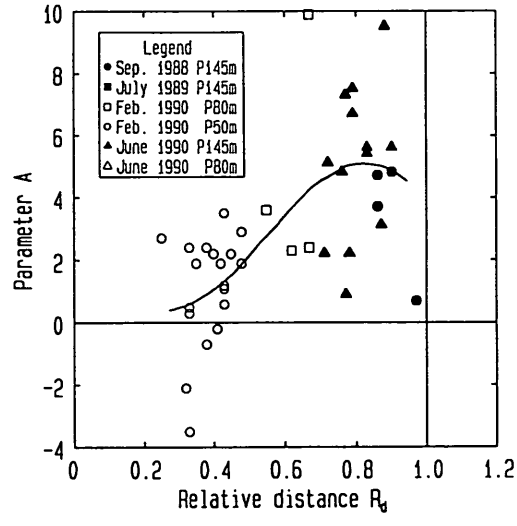

Fig.24(2) The relationship between the relative distance and the parameter A when R_P is 0.8

are the same. The data scatter around the solid line. However, there is a weak correlation between the value of A and the plunging breaker ratio in Fig.25 (1). Since the turbulence in a plunging breaking wave is larger than that in a spilling one (*Nadaoka and Kondoh*, 1982), the positive correlation between the value of A and the plunging breaker's ratio is recognized.

In Fig.25 (2), however, the value of A decreases as the ratio increases from 0.8 to 1.0, although the value of A increases as the ratio increases from 0.6 to 0.8. The region where the relative distance is 0.8 to 1.0 is the transition zone; *Nadaoka and*

Kondoh (1982) have defined that the transition zone is the region where a bore does not fully grow. Because the degrees of the bore growth are widely different in this zone, the value of A is mainly affected by the degree of bore growth. Consequently, the correlation between the value of A and the breaker type is poor in this region.

Although the relationship between the value of A and the bottom slope at the measurement station was investigated, a correlation could not be found out.

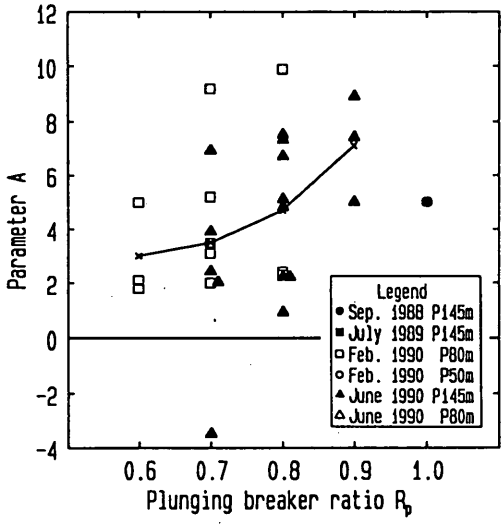

Fig.25(1) The relationship between the breaker type and the parameter A when R_d is from 0.6 to 0.8.

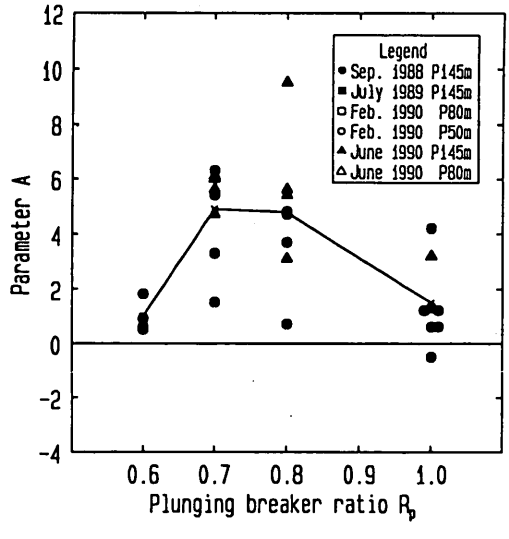

Fig.25(2) The relationship between the breaker type and the parameter A when R_d is from 0.8 to 1.0

5.2 Orbital velocities

The root-mean-square value of the orbital velocity along the principal wave direction, $(U_p)_{rms}$, can be predicted by Eq.(14) with the root-mean-square value of surface elevation. Equation (14) is derived with the small amplitude wave theory.

$$(U_p)_{rms,calc.} = \sigma \cdot \frac{\cosh k(h+z)}{\sinh kh} \eta_{rms} \quad , \tag{14}$$

where σ is the angular frequency, k is the wave number, and z is the location of an electro-magnetic current meter below the mean water level.

Figure 26 shows the comparison of the predicted velocities, $(U_p)_{rms,calc.}$, with the measured ones, $(U_p)_{rms,meas.}$. The measured values are about 0.8 times as much as the predicted ones. *Isobe* (1983) indicated that the ratio of the measured transfer function from the surface elevation to the horizontal particle velocity at the energy peak to that predicted with the small amplitude wave theory decreases as the wave height-water depth ratio increases. Concerning the root-mean-square value of the orbital velocity, however, the ratio is irrelevant to the wave height-water depth ratio, and is scattered around 0.8 as shown in Fig.27, where the wave height is $4\eta_{rms}$. The ratio was also investigated with respect to the wave nonlinearity parameter mentioned after; a correlation could not be found out.

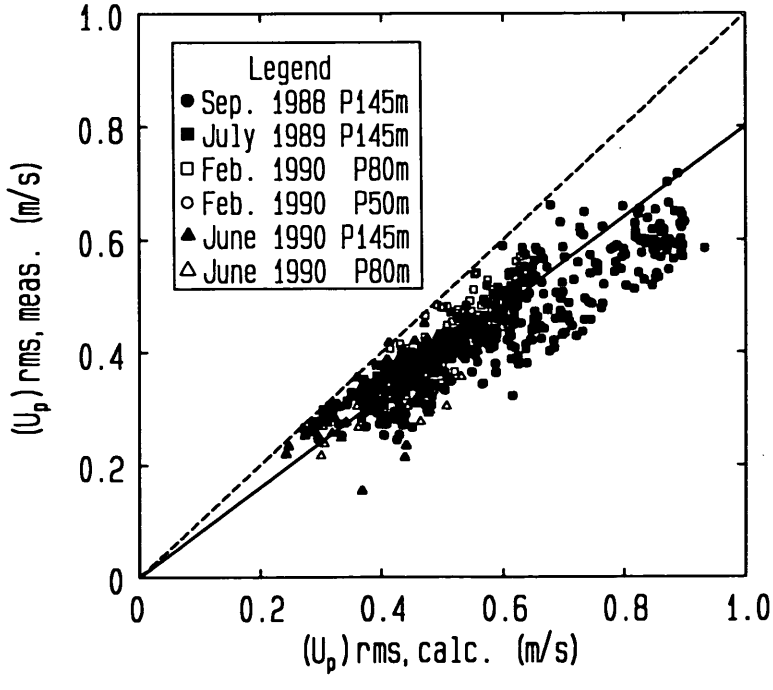

Fig.26 The comparison between the predicted root-mean-square value of the orbital velocity along the principal wave direction and the measured one

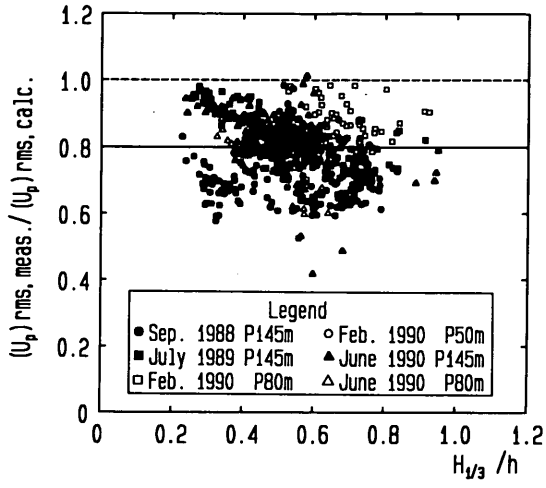

Fig.27 The relationship between wave height-water depth ratio and the ratio of the measured orbital velocity to the predicted one

5.3 Velocity atiltness

The atiltness of the velocity along the principal wave direction, $(\beta_3)_{U_p}$, which is expressed by Eq.(15), was plotted against the wave nonlinearity parameter Π in Fig.28.

$$(\beta_3)_{U_p} = -\left[\frac{1}{N-1}\sum_{i=1}^{N-1}\left((\dot{U}_p)_i - \bar{\dot{U}}_p\right)^3 \Big/ \left\{\frac{1}{N-1}\sum_{i=1}^{N-1}((\dot{U}_p)_i - \bar{\dot{U}}_p)^2\right\}^{3/2}\right]. \qquad (15)$$

Velocity atiltness is defined to be positive when the absolute values of the shoreward accelerations are larger than those of seaward accelerations, even though the velocity is defined to be positive in the seaward direction.

The wave nonlinearity parameter has been proposed by *Goda*(1983), and has been defined by Eq.(16).

$$\Pi = \frac{H}{L}\coth^3 kh\,. \qquad (16)$$

This parameter is equal to the wave steepness in deep water depth, and proportional to the Ursell number in shallow water depth. The parameter $\Pi_{1/3}$ is calculated with the significant wave height, for which the value of $4\eta_{rms}$ is used , and the small amplitude wavelength corresponding to the offshore significant wave period.

The velocity atiltness is strongly related to the wave nonlinear parameter as shown in Fig. 28. The velocity atiltness increases as the parameter increases within the measurement range, where the parameter is from 0.1 to 4.0.

The relationship between the atiltness of wave profile and the wave nonlinearity parameter is investigated in Appendix A for the study of the wave nonlinearity. Moreover, the wave profile skewness and the velocity skewness are discussed in Appendix B although they were not important for the cross-shore sediment transport rates in the surf zone.

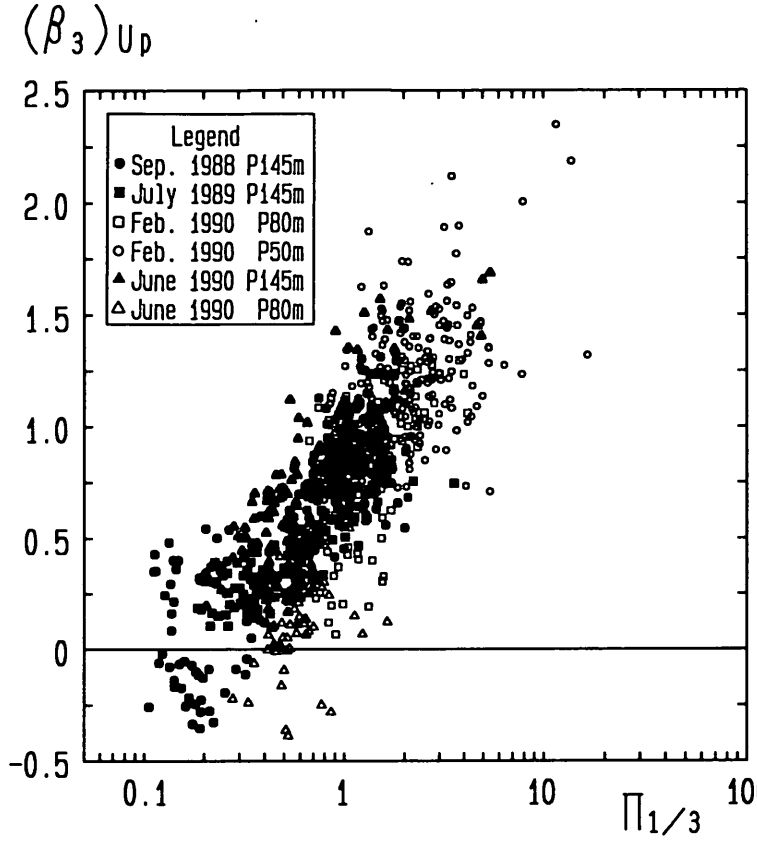

Fig.28 The relationship between $(\beta_3)U_p$ and $\Pi_{1/3}$

6. Summary

In order to investigate the relationships between the cross-shore sediment transport rates and the flow parameters in the surf zone, and in order to develop the prediction method for the flow parameters with the wave parameters, field measurements have been carried out in various wave conditions by using the HORF. The main conclusions are as follows:

(1) Time averaged cross-shore velocities, the root-mean-square values of the orbital velocities along the principal wave direction, and the forward asymmetry of the velocities affect the cross-shore sediment transport rates in the surf zone. The relationship between the cross-shore sediment transport rates and the flow parameters is expressed by Eq.(6), which consists of two terms. One represents the transport rate of the sediments which are suspended by the turbulence due to wave breaking and transported by the time-averaged cross-shore velocities. The rate is expressed by the product of the time-averaged cross-shore velocity, the water depth and the sediment concentration; the concentration is represented with the wave height-water depth ratio and one fourth of the Dean's number. The other term represents the sediment transport rate in the vicinity of ripples. The third power of the fluid acceleration is used in this term as the parameter to express the forward asymmetry of the velocity.

The new relationship expressed by Eq.(6) is valid not only near wave breaking

positions but also in the middle of the surf zone when the erosion volume in the foreshore is small. However, it cannot hold good even near the wave breaking positions when the erosion volume in the foreshore is large. The cause is considered to be that foreshore erosions occur through another mechanism of sediment transport, which is different from those considered in Eq.(6).

(2) The theoretical prediction formula for the time-averaged cross-shore velocity derived by *Svendsen* (1984) is improved for irregular waves with the introduction of the fraction of breaking waves and the root-mean-square value of water surface elevation. The improved formula, which is expressed by Eq.(9), is composed of two terms as Svendsen's model. One is the velocity due to surface variations and expressed by the right hand first term; it is verified with the field data outside the surf zone. The other is that due to the turbulence generated by wave breaking, which is expressed by the right hand second term. The surface roller area parameter A in Eq.(9) is related to the distance from wave breaking position to the measurement station and breaker type. The parameter A decreases as the distance increases. In the region where bores fully develop, the parameter A increases as the ratio of the plunging breakers to all breakers increases.

(3) The root-mean-square value of orbital velocity along the principal wave direction is 0.8 times as much as the velocity evaluated by Eq.(14), which is derived by the small amplitude theory, with the root-mean-square value of water surface elevation.

(4) The velocity atiltness is strongly related to the wave nonlinearity parameter proposed by *Goda* (1983). The atiltness increases as the parameter increases in the range from 0.3 to 4.

The conclusions have been obtained at a specific beach; for example, the medium sediment diameter is mostly 0.18mm. Therefore I hope that these conclusions are verified on the basis of the field data obtained from other beaches.

Acknowledgements

The author is grateful to Dr. Kazumasa Katoh, Chief of Littoral Drift Laboratory, Port and Harbour Research Institute, for his helpful suggestions and for his critical reading of the manuscript. The author also should like to express his thanks to Dr. Katsutoshi Tanimoto, Director of Hydraulic Engineering Division, Port and Harbour Research Institute and Dr. Okey Nwogu, Visiting Researcher of the Port and Harbour Research Institute (Research Associate, Hydraulics Laboratory Institute of Mechanical Engineering, National Research Council, Canada) for their critical reviews of the manuscript. Kashima Port Construction Office of the Second District Port Construction Bureau, Ministry of Transport, and Marine Observation Laboratory, Port and Harbour Research Institute, provided the offshore wave data. Finally, the author is grateful to Mr. Shin-ichi Yanagishima, Mr. Hiroyuki Murakami, Mr. Tomoyoshi Isogami and Mr. Satosi Nakamura, members of Littoral Drift Laboratory, and Mr. Tatsuo Usui and Mr. Takayuki Tsuchiya, members of ECOH Co., Inc., for their great contributions on the field measurements.

(*Received on March 18, 1991*)

References

1) Bagnold R.A. (1963): Mechanics of marine sedimentation, *The Sea, Ideas and Observations*, Vol.3, Intersience, New York, pp.507-528.
2) Bailard J.A. (1982): Modeling on-offshore sediment transport in the surf zone, *Proc. 18th Coastal Eng. Conf.*, ASCE, pp.1419-1438.
3) Bijker E.W., E.van Hijum and P.Vellinga (1976): Sand transport by waves, *Proc. 15th Coastal Eng. Conf.*, ASCE, pp.1149-1167.
4) Bowen A.J. (1980): Simple models of nearshore sedimentation, beach profiles and longshore bars, *The Coastline of Canada* (edited by S.B. MaCann), Geological Survey of Canada, pp.1-11.
5) Dally W.R. and R.G.Dean (1984): Suspended sediment transport and beach profile evolution, *J. Waterway, Port, Coastal and Ocean Eng.*, ASCE, Vol.110, No.1, pp.15-33.
6) Goda Y. (1975): Deformation of irregular waves due to depth-controlled wave breaking, *Rep. Port and Harbour Res. Inst.*, Vol.14, No.3, pp.59-106. (*in Japanese*)
7) Goda Y. (1983): A unified nonlinearity parameter of water waves, *Rep. Port and Harbour Res. Inst.*, Vol.22, No.3, pp.3-30.
8) Goda Y. (1985): Numerical examination of several statistical parameters of sea waves, *Rep. Port and Harbour Res. Inst.*, Vol.24, No.4, pp.65-102. (*in Japanese*)
9) Guza R.T. and E.B.Thornton (1985): Velocity moments in nearshore, *J. Waterway, Port, Coastal and Ocean Eng.*, ASCE, Vol.111, No.2, pp.235-256.
10) Irie I. and K.Nadaoka (1984): Laboratory reproduction of seabed scour in front of breakwaters, *Proc. 19th Coastal Eng. Conf.*, ASCE, pp.1715-1731.
11) Isobe M. (1983): Long period field observation on horizontal distribution of waves and currents in the nearshore zone, *NERC Rep.*, NO.17, TR-82-1, pp.17-34. (in Japanese)
12) Kajima R. and H.Katori (1988): Sediment transport rate, *Nearshore dynamics and coastal processes -theory, measurements and predictive models-* (ed. by K.Horikawa), University of Tokyo Press, pp.194-213.
13) Kana T.W. (1978): Surf zone measurements of suspended sediment, *Proc. 16th Coastal Eng. Conf.*, ASCE, pp.1725-1743.
14) Katoh K., N.Tanaka, T.Kondoh, M.Akaishi and K.Terasaki (1985): Field observation of local sand movements in the surf zone using fluorescent sand tracer (second report), *Rep. Port and Harbour Res. Inst.*, Vol.24, No.4, pp.3-63.
15) Katoh K., S.Yanagishima, Y.Kuriyama, T.Isogami, H.Murakami and M.Fujita (1990): Changes of grain distribution of bed material in the surf zone -Field observation at Hazaki Oceanographical Research Facility-, *Rep. Port and Harbour Res. Inst.*, Vol.29, No.2, pp.37-61. (*in Japanese*)
16) Nadaoka K., T.Kondoh and N.Tanaka (1982a): The structure of velocity field within the surf zone revealed by means of laser-doppler anemometry, *Rep. Port and Harbour Res. Inst.*, Vol.21, No.2, pp.49-106. (*in Japanese*)
17) Nadaoka K. and T.Kondoh (1982b): Laboratory measurements of velocity field structure in the surf zone by LDV, *Coastal Eng. Japan*, Vol.25, pp.125-146.
18) Nadaoka K., S.Ueno and T.Igarashi (1988): Field observation of three dimensional large-scale eddies and sediment suspension in the surf zone, *Coastal Eng. Japan*, Vol.31, No.2, pp.277-288.
19) Okayasu A., T.Shibayama and K.Horikawa (1988): Vertical variation of undertow in the surf zone, *Proc. 21st Coastal Eng. Conf.*, ASCE, pp.478-491.

20) Sasaki T. and K.Horikawa (1975): Nearshore current system on a gently sloping bottom, *Coastal Eng. Japan*, Vol.28, pp.123-142.
21) Sato S., M.Fukuhara and K.Horikawa (1988): Measurements of near-bottom velocities in random waves on a constant slope, *Coastal Eng. Japan*, Vol.31, No.2, pp.219-230.
22) Stive M.J.F. and Battjes J.A. (1984): A model for offshore sediment transport, *Proc. 19th Coastal Eng. Conf.*, ASCE, pp.1420-1436.
23) Stive M.J.F. (1986): A model for cross-shore sediment transport, *Proc. 20th Coastal Eng. Conf.*, ASCE, pp.1550-1564.
24) Sunamura T. (1980): An laboratory study of offshore transport of sediment and a model for eroding beaches, *Proc. 17th Coastal Eng. Conf.*, ASCE, pp.1051-1070.
25) Svendsen I.A. (1984): Mass flux and undertow in a surf zone, *Coastal Eng.*, 8, pp.347-365.

List of Symbols

a :third power of the fluid accerelation
A :surface roller area parameter
B_0 :wave shape parameter
C :wave celerity
$(E_A)_h$:error included in value A due to the error of h
$(E_A)_{P_b}$:error included in value A due to the error of P_b
$(E_A)_{\bar{v}}$:error included in value A due to the error of v
E_h :error in h
E_{P_b} :error in P_b
$E_{\bar{v}}$:error in $\bar{v}$
g :acceleration of gravity
h :water depth
H :wave height in general
$H_{1/3}$:significant wave height
k :wave number ($=2\pi/L$)
L :wavelength in general
P_b :fraction of breaking waves
Q :seaward sediment transport rate
$Q_{meas.}$:measured sediment transport rate
$Q_{calc.}$:predicted sediment transport rate
R_d :nondimensionalized distance between measurement station and shoreline divided with surf zone width
R_p :ratio of plunging breakers to all breakers
T :wave period in general
T_0 :offshore wave period
u :longshore velocity
U_p :velocity along the principal wave direction
$\dot{U}_p$:acceleration along the principal wave direction
$(U_p)_{rms}$:root-mean-square value of $(U_p-\overline{U_p})$
v :cross-shore velocity
$\bar{v}$:time-averaged seaward velocity
$\bar{v}_{wave}$:time-averaged velocity due to periodical surface variation
w_0 :fall velocity of sediment in sea water

z : location of an electro-magnetic current meter based on the mean water level

$(\sqrt{\beta_1})_\eta$: skewness of wave profile

$(\sqrt{\beta_1})_{U_p}$: skewness of velocity along the principal wave direction

$(\sqrt{\beta_1})_{U_p,S}$: skewness of short period component of velocity along the principal wave direction

$(\beta_3)_\eta$: atiltness of wave profile

$(\sqrt{\beta_3})_{U_p}$: atiltness of velocity along the principal wave direction

η : water surface elevation

η_{rms} : root-mean-square value of $(\eta-\overline{\eta})$

θ_p : principal wave direction

σ : angular frequency $(=2\pi/T)$

Π : wave nonlinearity parameter defined by Eq. (16)

Appendix A. Wave profile atiltness

The atiltness of wave profile was plotted as a function of the wave nonlinearity parameter in Fig.A.1. The wave profile atiltness increases as the parameter increases when the parameter is less than 3.0. When the parameter is more than 3.0, the atiltness does not seem to increase any more.

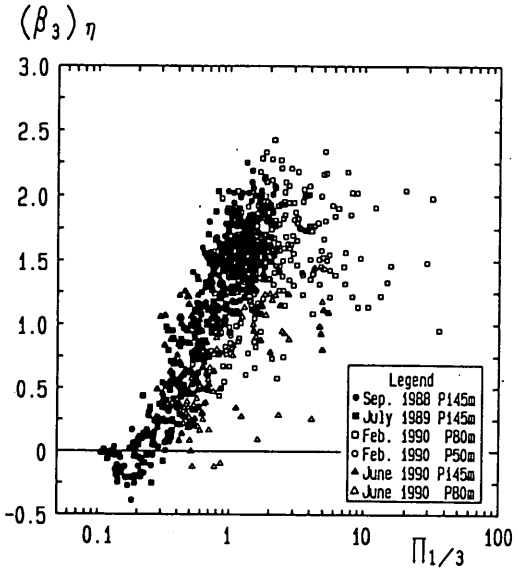

Fig.A.1 The relationship between $(\beta_3)_\eta$ and $\Pi_{1/3}$

Appendix B. Wave profile skewness and velocity skewness

The skewness, which is defined by Eq.(B1), represents the upward asymmetry of wave profile.

$$(\sqrt{\beta_1})_\eta = \frac{1}{N}\sum_{i=1}^{N}(\eta_i - \overline{\eta})^3 / \eta_{rms}^3 , \qquad \text{(B1)}$$

where $(\sqrt{\beta_1})_\eta$ is the skewness of wave profile.

The relationship between the wave profile skewness and the wave nonlinearity parameter can be represented by a parabola as shown in Fig.B.1. When the parameter is less than 1.0, the skewness increases as the parameter increases. When the parameter is more than 1.0, however, the skewness decreases with the increase of the parameter. This tendency has been also reported by *Goda* (1975) on the basis of the field data and the laboratory data with irregular waves.

Based on the laboratory data with regular waves, *Nadaoka et al.* (1982) concluded that the wave profile skewness has a peak at the breaking point, and that the peak skewness of the wave whose offshore wave steepness is small is larger than that of the wave whose steepness is large. In this investigation, however, the correlation between the distance from the wave breaking position to the measurement station and

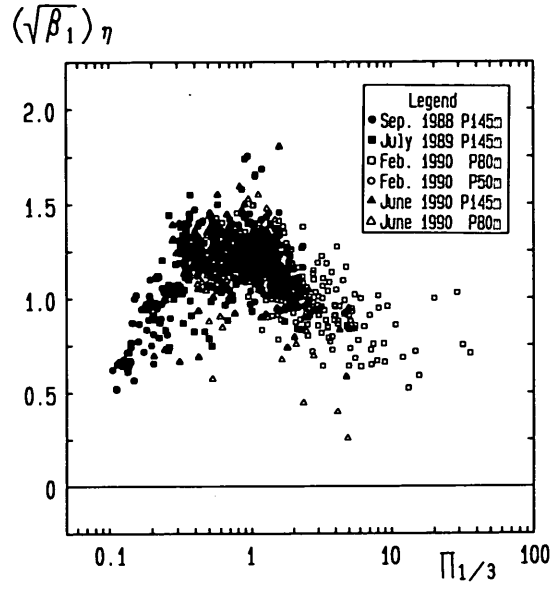

Fig.B.1 The relationship between $(\beta_3)_\eta$ and $\Pi_{1/3}$

the wave profile skewness during the visual observation is weaker than that between the wave nonlinearity parameter and the skewness. One of the reasons is that the skewness of irregular waves does not have a peak at the breaking position (*Sato et al.*, 1988). Another reason is that the wave height-water depth ratio in the wave nonlinearity parameter includes the effects of offshore wave steepness, bottom slope and the fraction of breaking waves. The wave height-water depth ratio in the surf zone increases as the offshore wave steepness increases or as the bottom slope steepens (*Goda*, 1975). The fraction of breaking waves has been expressed with the wave height-water depth ratio by *Thornton and Guza* (1983). Therefore the wave nonlinearity parameter including the wave height-water depth ratio is more suitable for representation of wave profile skewness than the distance from the wave breaking position to the measurement station.

Nadaoka et al. (1982) reported that the peak skewness depends on the offshore wave steepness, which is 0.01 to 0.07 in the experiment with regular waves. In the results with irregular waves by *Goda* (1975) and this study, however, the peak skewness is irrelevant to the offshore wave steepness. When waves are irregular and the values of offshore wave steepness are from 0.01 to 0.04, which are ordinarily observed in the field, the differences between the peak values of the skewness are small.

Figure B.2 shows the relationship between the skewness of the velocity along the principal wave direction and the wave nonlinearity parameter. The velocity skewness is smaller than the wave profile skewness. Although the relationship between the velocity skewness and the parameter can be indicated by a parabola, the values of velocity skewness are scattered more than the values of wave profile skewness. The cause is investigated in the consideration of infragravity waves.

Using the result of the spectral analysis, a time series of the velocities along the principal wave direction is divided into two components. One is the short period component, which is the sum of the decomposed waves whose wave periods are less than thirty seconds and the other is the long period component, which is the sum of the decomposed waves whose wave periods are greater than thirty seconds. The

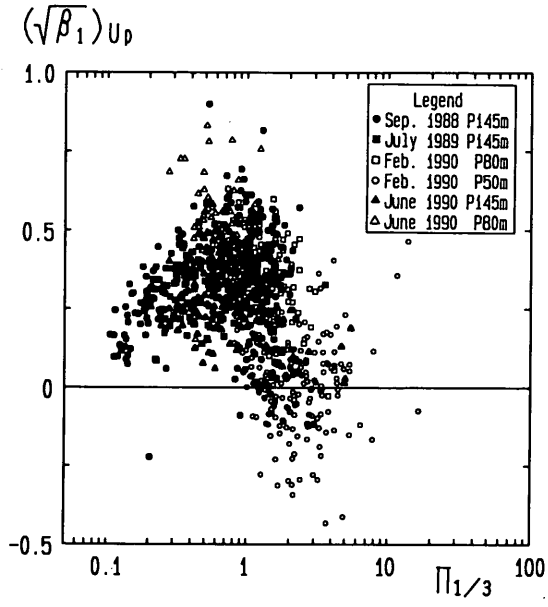

Fig.B.2 The relationship between $(\beta_3)_{Up}$ and $\Pi_{1/3}$

spectral analysis was carried out with the data for seventeen minutes; the number of the data is 2048 and the sampling frequency is 2Hz.

The relationship between the velocity skewness of the short period component, $(\sqrt{\beta_1})_{Up,S}$, and the wave nonlinearity parameter is shown in Figure B.3. The value of $(\sqrt{\beta_1})_{Up,S}$ is larger and less scattered than the value of $(\sqrt{\beta_1})_{Up}$. Hence it is considered that the scattering of the value of $(\sqrt{\beta_1})_{Up}$ is due to the infragravity waves.

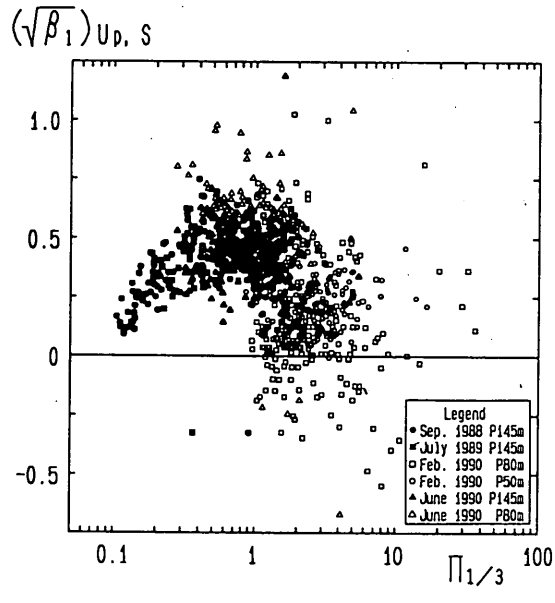

Fig.B.3 The relationship between $(\beta_3)_{Up,S}$ and $\Pi_{1/3}$